AWARD NUMBER:
W81XWH-17-1-0542

TITLE: Molecular crosstalk: bone metastatic prostate cancer and nociceptive neurons

PRINCIPAL INVESTIGATOR: Christopher Peters, Ph.D.

CONTRACTING ORGANIZATION: Wake Forest University Health Sciences

REPORT DATE: Oct 2019

TYPE OF REPORT: Annual report

PREPARED FOR: U.S. Army Medical Research and Materiel Command
Fort Detrick, Maryland 21702-5012

REPORT DOCUMENTATION PAGE

Form Approved
OMB No. 0704-0188

1. REPORT DATE	2. REPORT TYPE	3. DATES COVERED
Oct 2019	Annual	09/30/2018 - 09/29/2019

4. TITLE AND SUBTITLE
Molecular Cross-Talk: Bone Metastatic Prostate Cancer and Nociceptive Neurons

5a. CONTRACT NUMBER

5b. GRANT NUMBER
W81XWH-17-1-0542

5c. PROGRAM ELEMENT NUMBER

6. AUTHOR(S)

Yusuke Shiozawa, MD, PhD, Christopher Peters, PhD

E-Mail: yshiozaw@wakehealth.edu, chrpeter@wakehealth.edu

5d. PROJECT NUMBER

5e. TASK NUMBER

5f. WORK UNIT NUMBER

7. PERFORMING ORGANIZATION NAME(S) AND ADDRESS(ES)

Wake Forest University Health Sciences
Medical Center Blvd.
Winston-Salem NC 27157

8. PERFORMING ORGANIZATION REPORT NUMBER

9. SPONSORING / MONITORING AGENCY NAME(S) AND ADDRESS(ES)

U.S. Army Medical Research and Materiel Command
Fort Detrick, Maryland 21702-5012

10. SPONSOR/MONITOR'S ACRONYM(S)

11. SPONSOR/MONITOR'S REPORT NUMBER(S)

12. DISTRIBUTION / AVAILABILITY STATEMENT

Approved for Public Release; Distribution Unlimited

13. SUPPLEMENTARY NOTES

14. ABSTRACT

The goal of this project is to determine the roles of angiotensin II and its receptor in prostate cancer induced bone pain and bone metastatic growth. Aim 1 will provide the framework to identify the extent to which the interaction between cancer cells and nociceptive neurons through the angiotensin II and receptor axis affects cancer-induced bone pain. Aim 2 will determine the downstream molecular mechanisms whereby angiotensin II and its receptor axis affects bone pain. Aim 3 will define how nociceptive neuron influence tumor outgrowth. We believe that the insights derived from our investigations will lead to new strategies for reducing cancer-induced bone pain and also the outgrowth of bone metastasis.

During this period, we developed a syngeneic murine prostate cancer (PCa)-induced bone pain model which allows us to further elucidate the roles of the crosstalk between bone metastatic PCa and sensory neurons in both bone metastatic progression and its resultant bone pain in an immunocompetent setting. We developed an in vitro primary sensory neuron culture system to investigate the more detailed mechanism of the cancer/nerve interaction, and a semi-automated quantification method to measure the *in vitro* neurite outgrowth of these primary sensory neurons.

15. SUBJECT TERMS

Prostate Cancer; Bone metastasis; Disseminated tumor cells; Cancer-induced bone pain; Sensory nerves; Bone marrow microenvironment

16. SECURITY CLASSIFICATION OF:			17. LIMITATION OF ABSTRACT	18. NUMBER OF PAGES	19a. NAME OF RESPONSIBLE PERSON
a. REPORT	b. ABSTRACT	c. THIS PAGE			USAMRMC
Unclassified	Unclassified	Unclassified	Unclassified	37	19b. TELEPHONE NUMBER *(include area code)*

Table of Contents

1. INTRODUCTION:

Cancer-related pain, both its causes and its management, poses a tremendous challenge to patients and their caregivers. In the quest for effective cancer therapy, maintaining quality of life can be as crucial as treating the tumor. Seventy-five percent of cancer patients experience pain throughout the course of the disease, and once cancer metastasizes to the bone, the first symptom is often acute bone pain. A full 80% of patients with bone metastasis suffer from cancer-induced bone pain (**CIBP**). Current analgesic strategies for CIBP using nonsteroidal anti-inflammatory drugs (**NSAIDs**) and opioids are effective, but side effects, abuse, and addiction are serious and growing concerns associated with their use. It is therefore essential to develop therapeutic agents that can eradicate bone metastatic diseases and relieve resultant pain.

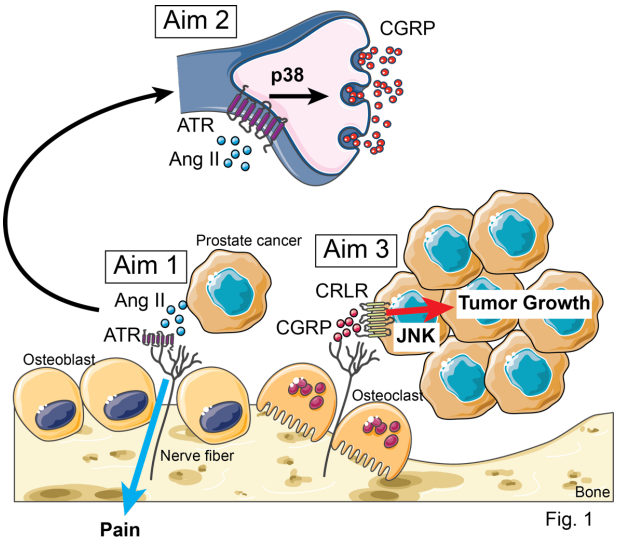

Fig. 1

Metastatic progression of disseminated tumor cells (**DTCs**) to bone may be environmentally directed by influences from the bone marrow microenvironment. Yet a full understanding of the more complex interactions that result in active bone marrow metastasis remains elusive. Our group recently discovered that early in the metastatic process, prostate cancer (**PCa**) cells target and commandeer the specific microenvironment for hematopoietic stem cells (**HSCs**), using mechanisms similar to those involved in HSC homing. Involvement of sympathetic and parasympathetic nerve fibers is crucial for both HSC maintenance and the dissemination of PCa to bone, suggesting that interactions between DTCs and nerves are at least in part responsible for controlling metastatic progression. However, the influence of sensory nerve fibers in the bone on PCa progression and metastasis has not been examined. Although it has been suggested that compression of the soft tissues or peripheral nerve fibers and interference with bone remodeling by bone tumors may be major causes of CIBP, little is known about the molecular interactions of DTCs with bone marrow nerve fibers, and how they affect CIBP.

Elucidating how these interactions influence CIBP is key. Angiotensin II (**Ang II**), a peptide that regulates blood pressure, is also involved in the progression of several types of cancer, including PCa. Ang II is pronociceptive in neuropathic and inflammatory pain models, and elicits sprouting of nociceptive neurons in the skin following inflammation through the angiotensin receptor (**ATR**). In a clinical study of several chronic musculoskeletal pain conditions, a small molecule inhibitor for ATR provided significant pain relief, suggesting that the Ang II/ATR axis controls pain signaling. Our preliminary data suggest that pain-associated neuropeptides can interact directly with PCa cells to cause enhanced proliferation. Therefore, it is critical to explore whether the Ang II/ATR axis is involved in the development of CIBP, and whether pain-associated neuropeptides regulate bone metastatic progression.

We hypothesize that **disseminated PCa stimulates sensory neurons that innervate bone through the Ang II/ATR axis; these cancer-associated sensory neurons then release neuropeptides, resulting in both CIBP and metastatic progression of PCa** (see **Fig. 1**). Ang II expressed by disseminated PCa induces CIBP (Aim 1) by stimulating sensory neurons to release calcitonin gene-related peptide (**CGRP**) through the ATR/p38 pathway (Aim 2). The nerve-derived CGRP enhances the growth of DTCs via its receptor calcitonin receptor-like receptor (**CRLR**) (Aim 3).

To address our hypothesis the following aims are proposed:

Aim 1: Determine how disseminated prostate cancer is involved in development of cancer-induced bone pain.

Aim 2: Define the intracellular signaling pathways in peripheral nerves stimulated by disseminated prostate cancer.

Aim 3: Determine the influence of nociceptive neurons on (a) tumor outgrowth in the bone and (b) cancer-induced bone pain.

The proposed studies will focus on fundamental mechanisms behind the novel concept that nerves in the bone marrow microenvironment have a crucial role in PCa bone metastasis. Aim 1 will provide the framework to identify the extent to which the interaction between DTCs and nociceptive neurons affects cancer-induced bone pain. Aim 2 will determine the molecular mechanisms of cancer-induced bone pain. Aim 3 will define how DTC/nociceptive neuron interactions influence tumor outgrowth. We believe that the insights derived from our investigations will lead to new strategies for reducing cancer-induced bone pain and also the outgrowth of DTCs. By promoting understanding of how the crosstalk between nociceptive neurons and DTCs participates in cancer-induced bone pain and tumor outgrowth, this study will lay the foundation for significant improvements in care of PCa patients, allowing development of pain targeting therapies that can also minimize bone metastatic progression. If successful, our study will not only shed new light on the fundamental mechanisms of PCa bone metastasis, but will quickly provide a gateway to novel treatment strategies to lower PCa-associated deaths and suffering, as some of the agents to be tested in this study have been in clinical trials for different diseases.

2. KEYWORDS:

Prostate Cancer; Bone metastasis; Disseminated tumor cells; Cancer-induced bone pain; Sensory nerves; Bone marrow microenvironment

3. ACCOMPLISHMENTS:

What were the major goals and objectives of the project?

The goal of this project is to determine the roles of the interaction between bone metastatic prostate cancer and sensory nerves in cancer-induced bone pain and bone metastatic growth.

Task 1: Determine whether Ang II expressed by disseminated tumor cells affects cancer-induced bone pain using pharmacological interference of Ang II and ATR interactions.

Months 1-11.

- Submit documents for local IACUC review (**Months 1-3; Dr. Shiozawa, Dr. Peters**).
- Submit IACUC approval and necessary documents for ACURO review (**Months 4-6; Dr. Shiozawa**).
- Design and develop an animal model to measure the tumor growth in the marrow, bone remodeling, and pain related behavior within the same animal (**Months 7-8; Dr. Shiozawa, Dr. Peters**).
- Test the effects of Ang II/ATR axis on the tumor growth in the marrow, bone remodeling, and pain related behavior within the same animal (**Months 9-11; Dr. Shiozawa, Dr. Peters**).

Task 2: Determine the effects of disseminated tumor cells on Ang II levels in the marrow and ATR expression in the dorsal root ganglia.

Months 12-14.

- Determine the kinetic pattern of Ang II levels in the tumor inoculated marrow and ATR expression in the tumor inoculated DRG (**Months 12-14; Dr. Shiozawa**).

Task 3: Determine the effects of Ang II expressed by disseminated tumor cells on cancer-induced bone pain by manipulating the tumor-nerve microenvironment.

Months 15-19.

- Design and develop nerve-specific ATR knockdown (KD) mice with adeno-associated viral vectors (**Months 15-16; Dr. Shiozawa, Dr. Peters**).
- Test the effects of Ang II/ATR axis on the tumor growth in the marrow, bone remodeling, and pain-related behavior within the same animal (ATR KD mice) (**Months 17-19; Dr. Shiozawa, Dr. Peters**).

Task 4: Determine whether the p38 pathway influences tumor growth, skeletal remodeling, and cancer-induced bone pain.

Months 20-22.

- Test the effects of p38 inhibitor on the tumor growth in the marrow, bone remodeling, and pain related behavior within the same animal (**Months 20-22; Dr. Shiozawa, Dr. Peters**).

Task 5: Determine the molecular mechanisms whereby Ang II expressed by disseminated tumor cells activates the bone marrow sensory nerves.

Months 23-24.

- Test the effects of ATR antagonist on the expression of pp38 and CGRP in DRG, spinal cord, and bone (**Months 23-24; Dr. Shiozawa, Dr. Peters**).

Task 6: Major Task 6: Define a link between Ang II expression by disseminated tumor cells with activation of the bone marrow sensory nerves in human subjects.

Months 1-34.

- Submit documents for local IRB review (**Months 1-3; Dr. Shiozawa**).
- Submit IRB approval and necessary documents for HRPO review (**Months 4-6; Dr. Shiozawa**).
- Clinical validation of results with bone biopsy samples of confirmed prostate cancer patients (**Months 7-34; Dr. Shiozawa, Dr. Peters**)
- Co-author manuscript on the effects of Ang II/ATR axis on the tumor growth, bone remodeling, and pain related behavior (**Months 23-26; Dr. Shiozawa, Dr. Peters**).

Task 7: Determine whether CGRP released from bone marrow sensory neurons influences tumor growth, skeletal remodeling, and cancer-induced bone pain.

Months 25-29.

- Design and develop nerve-specific CGRP knockdown (KD) mice with adeno-associated viral vectors (**Months 25-26; Dr. Shiozawa, Dr. Peters**).
- Establish CRLR KD PCa cells (**Months 25-26; Dr. Shiozawa**).

- Test the effects of CGRP/CRLR axis on the tumor growth in the marrow, bone remodeling, and pain-related behavior within the same animal (CGRP KD mice) (**Months 27-29; Dr. Shiozawa, Dr. Peters**).

Task 8: Determine whether CGRP promotes bone metastases through JNK pathway.

Months 30-31.

- Test the effects of CGRP antagonist on the expression of JNK in bone metastatic tumor (**Months 30-31; Dr. Shiozawa, Dr. Peters**).

Task 9: Determine whether JNK pathway influences tumor growth, skeletal remodeling, and cancer-induced bone pain.

Months 32-34.

- Test the effects of JNK inhibitor on the tumor growth in the marrow, bone remodeling, and pain related behavior within the same animal (**Months 32-34; Dr. Shiozawa, Dr. Peters**).

- Co-author manuscript on the effects of CGRP/CRLR axis on the tumor growth, bone remodeling, and pain related behavior (**Months 25-26; Dr. Shiozawa, Dr. Peters**).

- Co-author manuscript summarizing all the results (**Months 27-29; Dr. Shiozawa, Dr. Peters**).

What was accomplished under these goals?

(2017-2018)

Bone metastatic prostate cancer (PCa) causes enriches calcitonin gene-related peptide (CGRP)-expressing sensory nerves in the marrow, and that the CGRP/calcitonin receptor-like receptor (CRLR)/p38 pathway promotes PCa bone metastasis (Dr. Shiozawa).

CGRP downregulation in sensory nerves that innervate bone using adeno-associated virus serotype rh10 (AAVrh10) (Drs. Shiozawa and Peters).

(2018-2019)

Characterization of a syngeneic mouse model of prostate cancer-induced bone pain (Drs. Shiozawa and Peters).

As part of proposed studies, we developed and characterized a syngeneic mouse model of PCa-induced bone pain which has the advantage of allowing studies in immunocompetent animals which better reflect the normal bone microenvironment. Male C57BL6 mice were inoculated into the femur with murine RM-1 PCa cells ($1x10^3$ cells/5µL) or Hank's buffered saline as a sham control (**Fig. 1A**). Prior to injection, the RM-1 PCa line was transfected with luciferase reporters and green fluorescent protein (GFP) in order to visualize *in vivo* tumor growth longitudinally and quantify the extent of tumor burden at sacrifice. We observed a progressive increase in bioluminescence (BLI) in the ipsilateral hind limb of RM-1 but not sham mice between 7 and 21 days post-inoculation (**Fig. 1B&C**). Tumor induced bone remodeling, evident as cortical osteolytic lesions (**Fig. 1D&E & Fig. 2A&B**) and extra-periosteal aberrant bone formation (**Fig. 2C**), was observed in the ipsilateral femur of RM-1 but not sham mice based on histological and radiographic analysis.

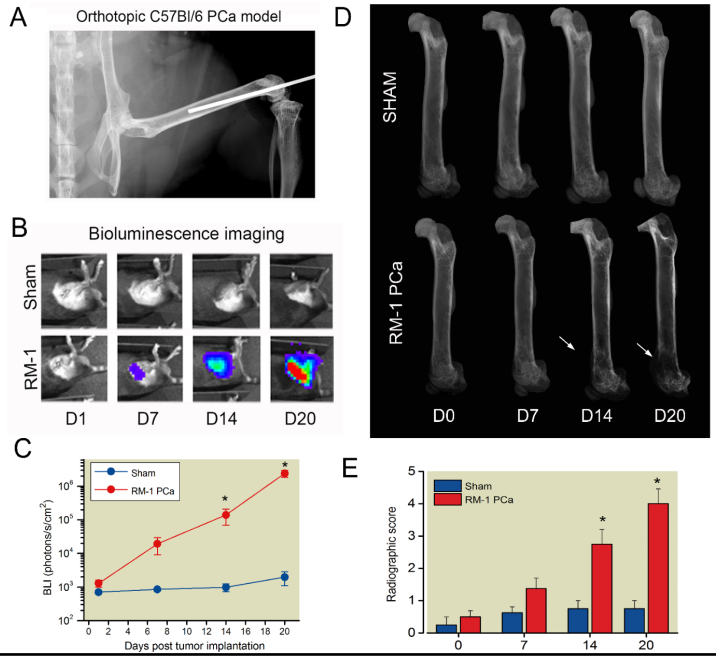

Figure 1: Development of an intra-femoral injection mouse model. C57Bl6 mice received intra-femoral injections of RM-1 PCa cells transduced with luciferase. Needle placement was verified radiographically (A). Tumor growth was monitored longitudinally with bioluminescence imaging (BLI) (B). Significant increases in BLI were observed 14 and 20 days post tumor cell inoculation (C). Longitudinal radiographs of ipsilateral femur from representative sham and RM-1 inoculated mice (D). Note osteolytic lesions present in distal femur (arrows) of tumor bearing mice. Quantification of pathological bone remodeling in sham and tumor bearing mice (E). Two-way RM ANOVA * $p<0.05$ versus within time point sham values. Sham n=7, RM-1 n=8.

Tumor growth was accompanied by spontaneous guarding of the inoculated limb suggestive of ongoing pain and impairment of daily running wheel performance indicative of movement evoked pain (**Fig. 3**). Additionally, spinal cord tissue was collected and examined immunohistochemically for markers of central sensitization. We found that tumor-inoculated mice had increased expression of dynorphin (**Fig. 4A&B**), pERK (**Fig. 4 C&D**) and GFAP (**Fig. 5A&B**) in the ipsilateral side of spinal cord. We also found the levels of CGRP and SP in terminal of sensory neurons within the spinal cord were significantly increased in tumor-inoculated mice, compared to sham mice (**Fig. 6**). The number of sensory (PGP9.5 +) nerve fibers was quantified in the periosteum, mineralized bone and bone marrow of tumor bearing and sham inoculated mice. Ectopic sprouting of sensory neurons was observed predominantly within the periosteum in close proximity to prostate cancer cells and regions of remodeled bone (**Fig. 7**). These results are being prepared in a manuscript for submission during the next funding cycle. Future studies will use this model in combination with transgenic Cre/Flpo driver mice to better understand sensory neuron tumor interactions that drive PCa induced bone pain and disease progression.

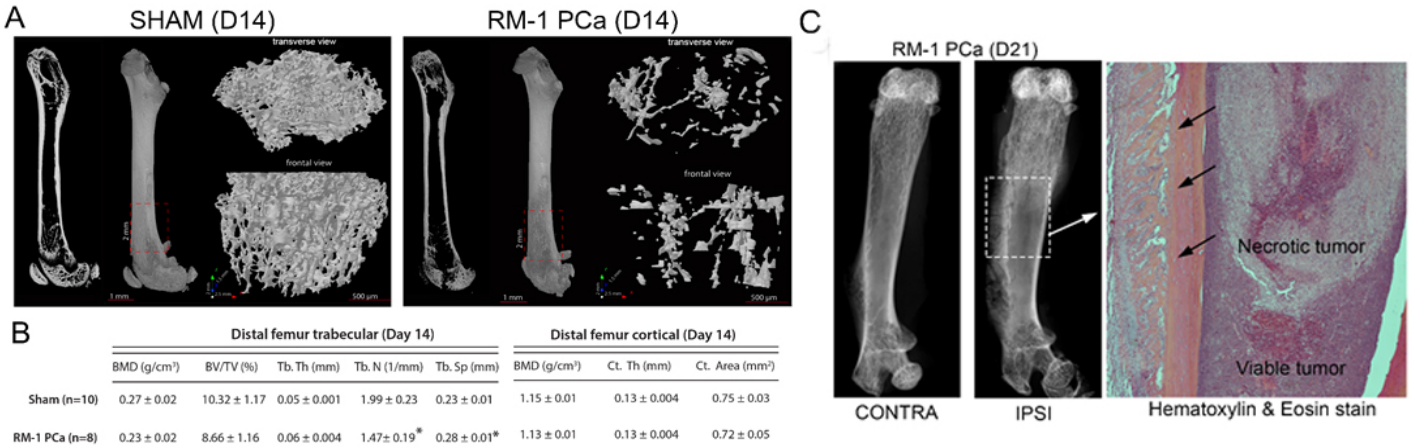

B

	Distal femur trabecular (Day 14)					Distal femur cortical (Day 14)		
	BMD (g/cm³)	BV/TV (%)	Tb. Th (mm)	Tb. N (1/mm)	Tb. Sp (mm)	BMD (g/cm³)	Ct. Th (mm)	Ct. Area (mm²)
Sham (n=10)	0.27 ± 0.02	10.32 ± 1.17	0.05 ± 0.001	1.99 ± 0.23	0.23 ± 0.01	1.15 ± 0.01	0.13 ± 0.004	0.75 ± 0.03
RM-1 PCa (n=8)	0.23 ± 0.02	8.66 ± 1.16	0.06 ± 0.004	1.47± 0.19*	0.28 ± 0.01*	1.13 ± 0.01	0.13 ± 0.004	0.72 ± 0.05

Figure 2. Assessment of bone morphrogy of mice inoculated into femur with PCa cells. µCT scans of femurs from sham and tumor bearing mice including 2D slice and 3D image of entire femur and distal metaphysis (insets, A). Quantification of key µCT outcomes (B) indicate loss of trabeculae due to osteolysis. Some tumor bearing mice develop extra-periosteal osteosclerotic lesions (black arrows) evident in radiographs and H&E at late stages (D21) of disease (C). Student's t-test *p<0.05 versus Sham values. Sham n=10, RM-1 n=8

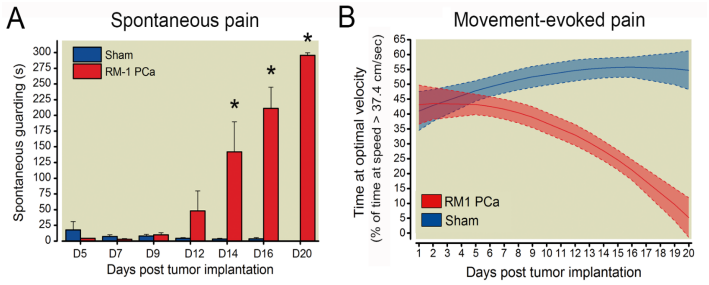

Figure 3. Assessment of pain behaviors of mice inoculated into femur with PCa cells. Time course of ongoing or spontaneous pain in mice following intra-femoral-injection of RM-1 PCa cells or sham injections is evident as progressive increase in duration of guarding of the tumor bearing hindlimb (A). Two-way RM ANOVA with Bonferroni comparisons *P<0.05 versus sham values within time point. Sham n=8, RM-1 n=9. Tumor bearing mice also displayed progressive impairment in the time spent running at an optimal velocity during daily 30 minute sessions compared to sham mice (B) potentially reflecting movement evoked pain or cancer induced functional disability. Longitudinal running wheel data best fit a quadratic form. Mice inoculated with RM-1 demonstrated a significantly decelerating trajectories (Time^2 X Group, p= 0.003) but similar intercepts (Group, p= 0.65). Sham n= 12, RM-1 n=12.

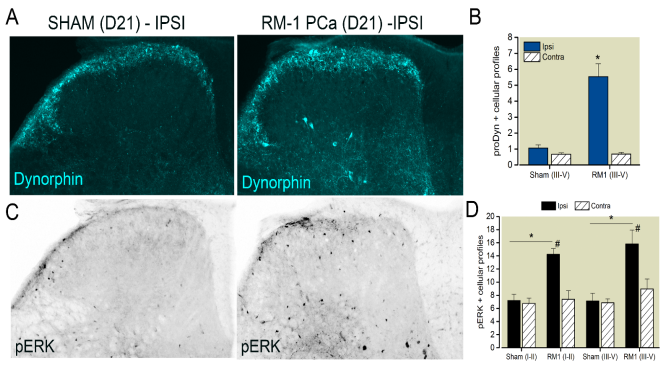

Figure 4.Central sensitization is observed in the ipsilateral spinal cord of PCa inoculated mice. Spinal cord of tumor bearing mice 21 days post inoculation. Representative images of proDynorphin-IR (A) and pERK-IR (C) in the ipsilateral spinal cord of sham and RM-1 PCa inoculated mice. Dynorphin-IR cellular profiles are increased in the ipsilateral deep dorsal horn of tumor bearing mice (B) pERK-IR profiles are increased in superficial and deep dorsal horn of tumor bearing mice (D). Two way ANOVA with Bonferroni comparisons * p<0.001 vs. sham. # p<0.05 vs. contra values. Sham n=8, RM-1 n=8.

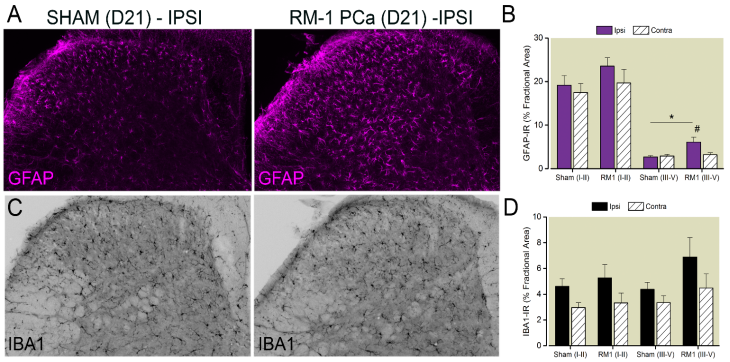

Figure 5. Enhanced glial activation is present in the ipsilateral spinal cord of tumor bearing mice. Alterations in glial plasticity were assessed with antibodies against GFAP for astrocytes (A) and IBA1 for microglial (C) in the ipsilateral spinal cord of tumor bearing mice 21 days post inoculation. GFAP-IR is increased in the ipsilateral deep dorsal horn of tumor bearing mice (B). IBA1-IR was not significantly greater in tumor bearing vs sham mice, however there was a general increase in IBA1-IR in the ipsilateral side. Two way ANOVA with Bonferroni comparisons *p<0.001 vs sham, # p<0.05 vs. contra. Sham n=8, RM-1 n=8.

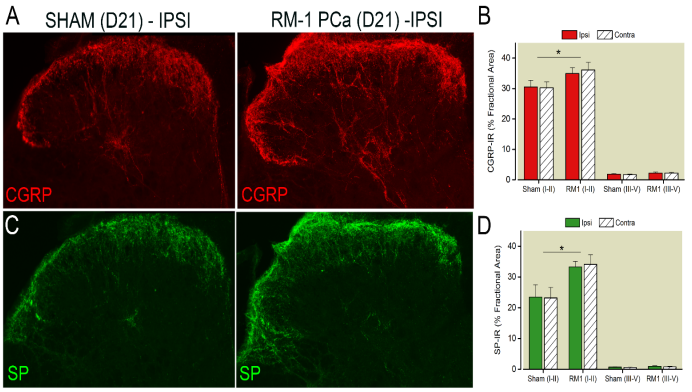

Figure 6.Increased levels of neuropeptides CGRP and SP are present in the spinal cord of tumor bearing mice. Alterations in density of calcitonin gene related peptide (CGRP, A) and substance P (SP, C) in terminals of sensory neurons within the lumbar spinal cord of sham and tumor bearing mice. CGRP-IR (B) and SP-IR was increased bilaterally in superficial dorsal horn of tumor bearing mice. Two way ANOVA with Bonferroni comparisons *p<0.001 vs sham

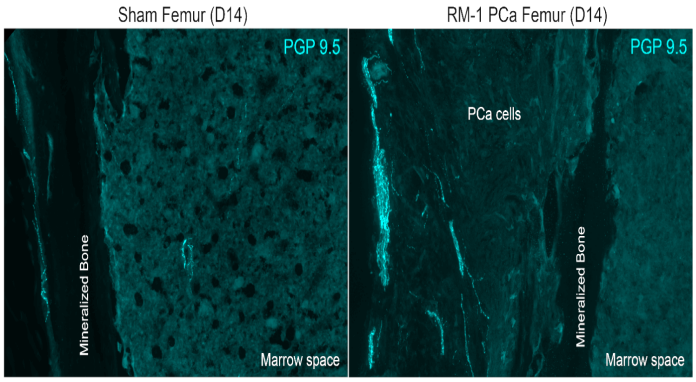

Figure 7. Characterization of sensory neurons in the bone of mice inoculated into femur with PCa cells. Sections of the mouse femur were immunohistochemically labeled with an antibody against PGP 9.5 to assess changes in nerve fiber density within the bone. Fourteen days after inoculation, sham mice have nerve fibers within the periosteum lining the mineralized bone and within the bone marrow. In RM-1 tumor bearing mice, there is a reduction in nerve fibers within the marrow space but a robust sprouting of neurons adjacent to tumor cells that have invaded through the mineralized bone into the periosteum.

Cancer-derived factors stimulated the neurite outgrowth of murine sensory neurons (Dr. Shiozawa).

To establish a primary 2D DRG neuron culture, L2-4 DRGs were collected from C57BL/6 mice and dissociated them into single cell suspension by enzymatic digestion. The resulting DRGs were plated onto poly-D-lysine/laminin-coated coverslips and cultured in neuronal growth media. Unlike other studies, DRGs were maintained in serum free of nerve-related growth factors (e.g. NGFs, GDNFs) to avoid their influence on the survival of neurons and neurite outgrowth. As shown in **Fig. 8A**, cells obtained from DRGs, including sensory neurons and satellite cells, were viable for at least 15 days in serum and growth factor-free conditions. Although approximately 90% of sensory neurons extended neurites, it was very difficult observe under the light microscope since multiple cell types overlapped with each other. To visualize sensory neuron subsets, DRGs were stained with DAPI and three different neuronal markers: 200 kD neurofilament (NF200, typically myelinated A fibers; calcitonin gene-related peptide (CGRP, typically peptidergic myelinated Aδ or

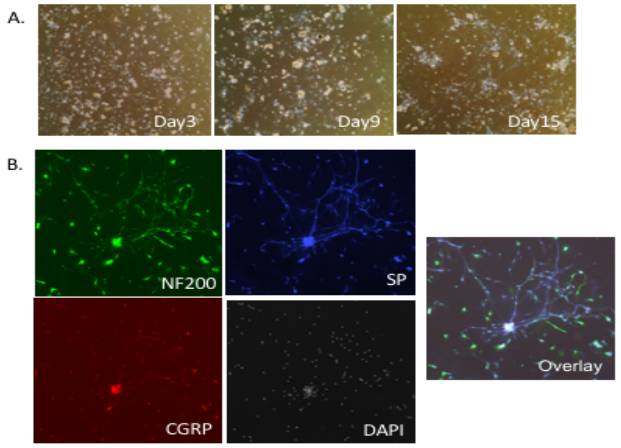

Figure 8. Establishment of a murine primary 2D DRG neuron culture.

(**A**) Representative bright field images of murine primary DRG culture seeded onto Poly-D-lysine/laminin coated coverslips at Day 3, 9, and 15. (**B**) Representative immunofluorescence images of (A) at Day 15. Sensory neurons were stained with antibodies against NF200 (green), CGRP (red), and Substance P (blue). DAPI (gray) is used for nuclear staining. Magnification 10x.

To further confirm whether cells in pellet fraction were sensory neurons, they were stained with neuronal markers NF200, CGRP, and IB4 (non-peptidergic unmyelinated C-fibers). Interestingly, NF200 positive neurons always co-localized with CGRP positive neurons, but not IB4 positive neurons (**Fig. 10A**). Additionally, some CGRP positive neurons overlapped with IB4 positive neurons (**Fig. 10A**). Moreover, the size of soma was arbitrarily divided into small (< 600 μm^2), medium (600-1,200 μm^2) and large (1,200-3,000 μm^2). Small (28%); medium (44%); and large (28%) size neurons consisted of NF200 negative/CGRP negative/IB4 positive neurons; NF200 negative/CGRP positive/IB4 positive, NF200 negative/CGRP positive/IB4 negative, or NF200 positive/CGRP positive/IB4 negative neurons; and NF200 positive/CGRP positive/IB4 negative neurons, respectively (**Fig. 10B**).

Next, to test whether the growth of sensory neurons can be manipulated *in vitro* by exosome unmyelinated C fibers); substance P (SP, peptidergic unmyelinated C-fibers). Sensory neurons as well as their associated neurites expressed these markers, whereas satellite cells failed to do so (**Fig. 8B**).

It has been demonstrated that, in the peripheral nerve system, satellite cells are involved in the regulation of survival and axonal growth of neurons. Since one of our main purposes of establishment of primary DRG neuronal culture is to investigate the direct effects of exogenous factors on the neurite outgrowth of sensory neurons, our next attempt was to separate sensory neurons from satellite cells. To do so, density gradient centrifugation was performed using 3.5% BSA solution. After purification, sensory neurons were enriched in pellet fraction, while satellite cells were concentrated in the BSA layer. When cells in pellet fraction were plated, the numbers of satellite cells (S100 positive) were reduced, compared to before purification (**Fig. 9A**). To further confirm the quality of purification, both cells in pellet fraction and BSA layer were plated. As expected, cells in pellet fraction could extend neurites, while cells in BSA layer failed to so (**Fig. 9B**).

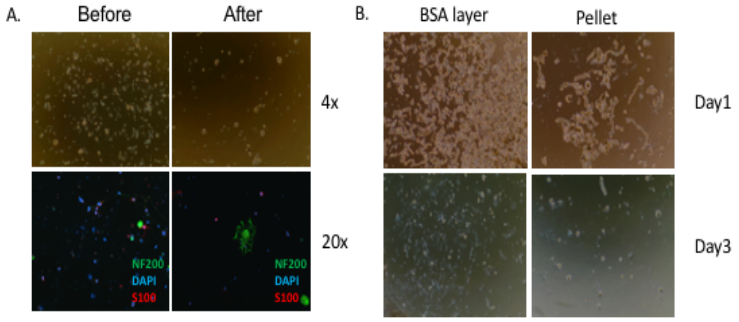

Figure 9. Purification of murine primary DRG sensory neurons using a BSA gradient centrifugation.

(**A**) DRG cells were seeded onto Poly-D-lysine/laminin coated coverslips before or after a BSA gradient centrifugation. Representative bright field images of murine DRGs before and after a BSA gradient centrifugation (top panels). Representative immunofluorescence images murine DRGs before and after BSA centrifugation (bottom panels). Sensory neurons were stained with antibodies against NF200 (green), and satellite cells were stained with antibodies against S100b (red), DAPI (blue) is used for nuclear staining. Magnification 20x. (**B**) After a BSA gradient centrifugation, cells obtained from the pellet fraction (pellet) and BSA layer were seeded onto Poly-D-lysine/laminin coated coverslips. Representative bright field images of cells from the pellet fraction and BSA layer at Day 1 (top panels) and 3 (bottom panels). Magnification 4x

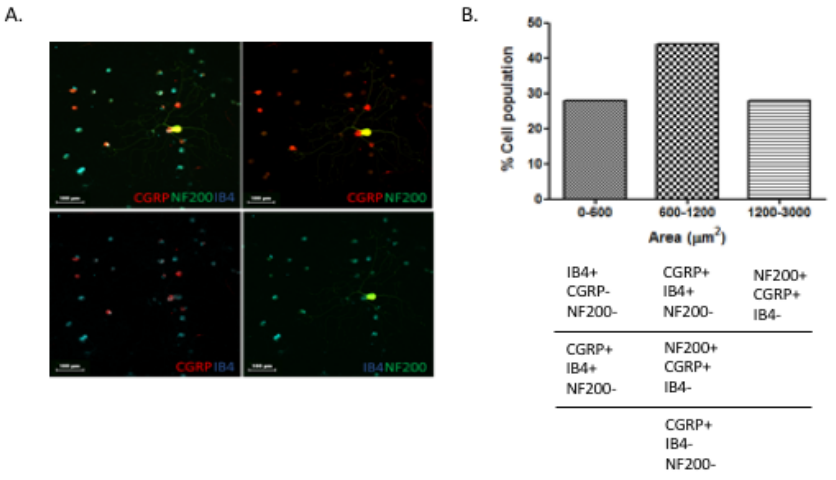

Figure 10. Characterization of murine primary DRG sensory neurons. (**A**) Representative IHC images of murine primary DRG sensory neurons after a BSA gradient centrifugation. Sensory neurons were stained with antibodies against NF200 (Green), CGRP (red), and IB4 (light blue). Magnification 4x. (**B**) Quantification analysis of the cell size distribution of murine primary DRG sensory neurons. Areas of soma (μm^2) of cells from (A) were measured using image J software.

factors, murine primary sensory neurons were treated with cancer-derived conditioned medium (CM). When sensory neurons were exposed to CM derived from the prostate cancer cell line DU145 cells, the density and average length of neurites from sensory neurons significantly increased compared to those exposed to control CM (**Fig. 11A&B**).

For quantification of neurite outgrowth, we used a commercially available image analysis software, Visiopharm to automatically measure a total neurite length and Image J to count the numbers of the soma in each coverslip. Then, a total neurite length was normalized with soma count. To validate whether an automated method can accurately be used to analyze neurite outgrowth, we first created a novel algorithm (called an "APP") using Visiopharm that enable us to detect the somas and measure the length of their neurites based on structural differences and fluorescence intensity, respectively (**Fig. 12A**). Then, values obtained automatically (Visiopharm) were compared to those obtained manually (Image J). As shown in **Fig. 12B**, total neurite lengths obtained using these two different methods were highly correlated (r^2=0.8975). However, soma counts were not as highly correlated as total neurite lengths (r^2=0.1561) (**Fig. 12C**). This might in part be due to the difficulty to segregate the cluster of the somas into a single soma. Since (i) the total neurite length obtained using an automated method were similar to that obtained manually; (ii) a manual counting method provided more accurate information regarding the numbers of soma than an automated method; and (iii) by manually, counting somas was not as time consuming as measuring neurite length, we chose the quantification strategy described above.

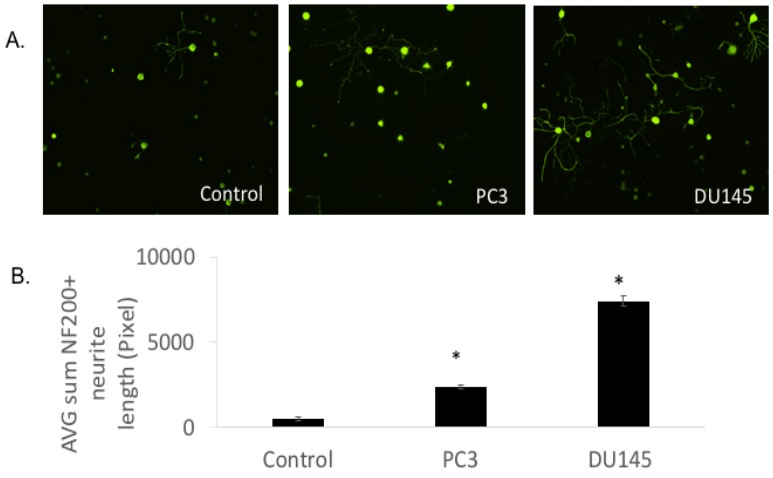

Figure 11. Sprouting of murine primary DRG sensory neurons by exogenous tumor derived factors.

(**A**) Representative immunofluorescence images of murine primary DRG sensory neurons treated with either control or PCa cell (DU145 and PC3)-derived conditioned media (CM) (0% serum) for 48 h. Sensory neurons were stained with antibodies against NF200. Magnification 4x. (**B**) Quantification of the average of the total neurite length per image of (A): Student's *t*-test

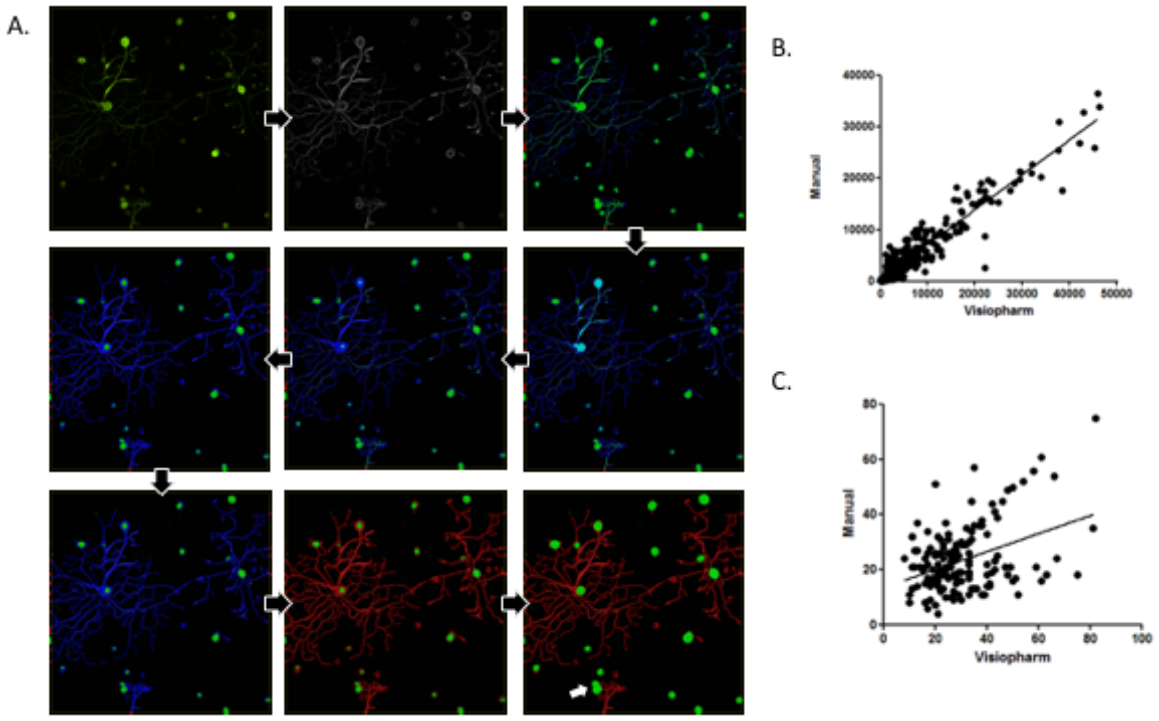

Figure 12. Quantification of total neurite length by manual versus automated imaging analysis.

(**A**) Representative images of the image-processing steps performed in the Visiopharm APP used for automated neurite length quantification and soma count, starting from the original fluorescent image of NF200 stained mouse DRG neurons (top left) to the final quantified image (bottom right) with relevant masks for neurite length (red) and soma count (green). Black arrow: direction of processing steps. White arrow: two neurons inaccurately counted as one. (**B**) 316 images of murine primary DRG sensory neurons stained with antibodies against NF200 were analyzed using the Visiopharm APP and by manual tracing using ImageJ software. Values for total neurite length were plotted (μm): Linear regression analyses. (C) 164 images of murine primary DRG sensory neurons stained with antibodies against NF200 were analyzed using the Visiopharm APP and by manual counting using ImageJ software and values for total soma numbers were plotted (counts): Linear regression analyses.

What opportunities for training and professional development did the project provide?

(2017-2018)
Dr. Shiozawa was invited to give a seminar at Jikei University School of Medicine (Tokyo, Japan) on October 11, 2017.

Dr. Peters organized a symposium at Wake Forest University Medical School entitled "*Translational Cancer Pain Research: Bridging the Gap Between Basic Science and Clinical Application* ". The symposium consisted of presentations from 3 clinicians (Dr. Francis Walker, Dr. Glenn Lesser, Dr. Roy Strowd) who specialize in clinical research focused on interventional studies for the treatment of cancer related pain and sensory dysfunction as well as 2 preclinical researchers (Dr. Chris Peters, Dr. Mario Danelo Boada) who are conducted mechanistic research studies in rodent models of cancer pain. The keynote speaker was Dr. Patrick Dougherty from MD Anderson Cancer Center who presented a lecture entitled "Inflammation and Ectopic Spontaneous Activity: New Findings of Chemotherapy Induced Peripheral Neuropathy in Humans &

Animals". This symposium came about largely as a result of the collaborative efforts driven by Dr. Shiozawa between clinicians within Wake Forest Comprehensive Cancer Center and faculty members within the Department of Anesthesiology at Wake Forest Baptist Medical Center.

(2018-2019)
Dr. Shiozawa was invited to give a talk at The U.S. Bone and Joint Initiative (USBJI) and Bone and Joint Canada (BJC) Young Investigator Initiative Workshop Spring 2019 (Rosemont, IL) on April 27, 2019.

Dr. Shiozawa was invited to give a seminar at University of North Carolina at Chapel hill, Adams School of Dentistry (Chapel hill, NC) on December 03, 2019.

Dr. Peters presented a poster at Neuroscience 2019 the Annual Society for Neuroscience Meeting in Chicago, Illinois October 19th-23, 2019.

How were the results disseminated to communities of interest?

There is nothing to report at this time.

What do you plan to do during the next reporting period to accomplish the goals and objectives?

In the next year of the award, we will continue to determine the roles of renin-angiotensin system in PCa-induced bone pain (Aim 1). We will also further elucidate the molecular mechanisms whereby bone metastatic PCa stimulates sensory nerves (Aim 2). In addition, we will continue to pursue studies examining the effects of sensory nerves on the progression of bone metastatic PCa (Aim 3).

4. IMPACT:

What was the impact on the development of the principal discipline(s) of the project?

(2017-2018)

We found that PCa enhances the sprouting of CGRP-expressing sensory nerves both in vitro and in vivo.

We found that PCa patients with bone metastases have high levels of CGRP in their serum, that PCa in bone metastatic sites expresses high levels of CRLR, and that CRLC expression levels in PCa is associated with their recurrent free survival.

We found that CGRP induces PCa proliferation through CRLR/p38 pathway.

We developed the technique to manipulate gene expression in sensory nerves innervating bones using an AAVrh10 virus vector.

(2018-2019)

We developed a syngeneic murine cancer-induced bone pain model which allows us to further investigate the mechanisms how bone metastatic PCa influence bone pain behaviors in an immunocompetent setting. Future studies will use this model in combination with transgenic Cre/Flpo driver mice to better understand sensory neuron tumor interactions that drive PCa induced bone pain and disease progression.

We established an *in vitro* sensory neuron culture system to further study interaction between PCa and sensory neurons.

We developed a semi-automated quantification method to measure the *in vitro* neurite outgrowth of sensory neurons.

What was the impact on other disciplines?

There is nothing to report at this time.

What was the impact on technology transfer?

There is nothing to report at this time.

What was the impact on society beyond science and technology?

There is nothing to report at this time.

5. CHANGES/PROBLEMS:

Changes in approach and reasons for change

Nothing to report.

Actual or anticipated problems or delays and actions or plans to resolve them

Nothing to report.

Changes that have a significant impact on expenditures

Nothing to report.

Significant changes in use or care of human subjects, vertebrate animals, biohazards, and/or select agents

Nothing to report.

6. PRODUCTS:

Publications, conference papers, and presentations

Journal Publications

Peer reviewed journal

(2017-2018)

1. Park SH, Eber MR, Tsuzuki S, Booker ME, Sunil AG, Widner DB, Parker RA, **Peters CM**, **Shiozawa Y**. Adeno-associated virus serotype rh10 is a useful gene transfer vector for sensory nerves that innervate bone in immunodeficient mice. **Sci Rep**. 2017;7:17428. PMID: 29233995. PMCID: PMC5727257.
   Status of Publication: Published
   Acknowledgement of federal support: Yes

   - **Selected as Papers of the Week (9 Dec 2017- 15 Dec 2017) by Pain Research Forum**

(2018-2019)

2. Jones JD, Sinder BP, Paige D, Soki FN, Koh AJ, Thieleb S, **Shiozawa Y**, Hofbauer LC, Daignault S, Roca H, McCauley LK. Trabectedin reduces skeletal prostate cancer tumor size in association with effects on M2 macrophages and efferocytosis. **Neoplasia**. 2018;21:172-184. PMID: 30591422. PMCID: PMC6314218.
   Status of Publication: Published
   Acknowledgement of federal support: Yes

Invited reviews

(2017-2018)

1. Park SH, Keller ET, **Shiozawa Y**. Bone marrow microenvironment as a regulator and therapeutic target for prostate cancer bone metastasis. **Calcif Tissue Int**. 2018;102:152-62. PMID: 29094177. PMCID: PMC5807175.
   Status of Publication: Published
   Acknowledgement of federal support: Yes

2. Widner DB, Files DC, Weaver KE, **Shiozawa Y**. Preclinical and clinical studies on cancer-associated cachexia. **Front Biol**. 2018;13:11-18. PMID: In Progress. PMCID: In Progress.
   Status of Publication: Published
   Acknowledgement of federal support: Yes

3. Park SH, Eber MR, Widner DB, **Shiozawa Y**. Role of the bone microenvironment in the development of painful complications of skeletal metastases. **Cancers (Basel)**. 2018;10:141. PMID: 29747461. PMCID: PMC5977114.
   Status of Publication: Published
   Acknowledgement of federal support: Yes

   - **Selected as Featured Paper**

4. Widner DB, Park SH, Eber MR, **Shiozawa Y**. Interactions between disseminated tumor cells and bone marrow stromal cells regulate tumor dormancy. **Curr Osteoporos Rep**. 2018;16:596-602. PMID: 30128835. PMCID: In Progress.
   Status of Publication: Published
   Acknowledgement of federal support: Yes

   (2018-2019)

   Nothing to report.

Book

(2017-2018)

1. Park SH, Eber MR, **Shiozawa Y**. (2018) Tumor inoculation mouse models of prostate cancer bone metastasis. In Idris A (Ed.), *Bone Research Protocols - 3rd Edition.* In Press. London: Springer Nature.
   Status of Publication: Accepted
   Acknowledgement of federal support: Yes

2. Park SH, Eber MR, Taichman RS, **Shiozawa Y**. (2018) Determining Competitive Potential of Bone Metastatic Cancer Cells in the Murine Hematopoietic Stem Cell Niche. In Turksen K (Ed.), *Stem cells and Niche - 2nd Edition: Methods and Protocols*, Methods in Molecular Biology. In Press. New York: Humana Press. Methods Mol Biol. In Press. PMID: 30099699. PMCID: In Progress.
   Status of Publication: Published
   Acknowledgement of federal support: Yes

   (2018-2019)

3. Park SH, **Shiozawa Y**. (2019) Genomic mutation as a potential driver of the development of bone-related cancers. In Zaidi M (Ed.), *Encyclopedia of Bone Biology*. In Press. Elsevier.
   Status of Publication: In Press
   Acknowledgement of federal support: Yes

4. **Shiozawa Y**. (2019) The roles of bone marrow-resident cells as a microenvironment for bone metastasis. In Birbrair A (Ed.), *Tumor Microenvironments in Different Organs – Part A*. In Press. Switzerland: Springer Nature.
   Status of Publication: In Press
   Acknowledgement of federal support: Yes

Presentation

(2017-2018)

1. Williams SN, Eber MR, Tsuzuki S, Park SH, **Shiozawa Y**. Does histamine influence the osteoblastic activities that help regulate the progression of bone metastatic prostate cancer? The 2017 Annual Biomedical Research Conference for Minority Students (ABRCMS), Phoenix, AZ, USA, November 1-4, 2017. Poster.

(2018-2019)

2. Lycan T, Thomas A, Hsu FC, Cartwright MS, Walker FO, Ahn C, Sangueza OP, **Shiozawa Y**, Park SH, **Peters CM**, Melin SA, Avery TP, Sorscher S, Lesser GJ, Strowd RE. Neuromuscular ultrasound for assessment of peripheral neuropathy in breast cancer patients receiving taxane therapy. J Clin Oncol 36, 2018 (suppl; abstr e22083). 2018 American Society Of Clinical Oncology (ASCO) Annual Meeting, Chicago, IL, USA, June 1-5, 2018. Poster.

3. Strowd RE, Lycan T, Thomas A, Hsu FC, Ahn C, Sangueza O, **Shiozawa Y**, Park SH, **Peters CM**, EA Romero-Sandoval, Melin SA, Sorscher S, Lesser GJ, Walker FO, Cartwright MS. Neuromuscular ultrasound for the non-invasive assessment of breast cancer patients with peripheral neuropathy from taxanes. The American Academy of Neurology 71st Annual Meeting, Philadelphia, PA, USA, May 4-10, 2019. Poster.

4. Tsuzuki S, Park S, Eber M, Widner B, Kamata Y, Kimura T, Bianchi-Frias D, Coleman I, Nelson P, Hsu F-C, **Peters C**, **Shiozawa Y**. A pain-related neuropeptide calcitonin gene-related peptide promotes bone metastatic progression of prostate cancer through p38. American Society for Bone and Mineral Research (ASBMR) 2019 Annual Meeting, Orland, FL, USA, September 20-23, 2019. Poster.

5. Park S, Eber M, Tsuzuki S, Cain R, Widner B, Kamata Y, Kimura T, Bianchi-Frias D, Coleman I, Nelson P, Hsu F-C, **Peters C**, **Shiozawa Y**. The role of the SCF/c-kit pathway in cancer-induced bone pain. American Society for Bone and Mineral Research (ASBMR) 2019 Annual Meeting, Orland, FL, USA, September 20-23, 2019. Poster.
   - **Selected as a Plenary Poster**

6. Cain R, Park SH, Eber M, Martin TJ, Parker R, Jimenez-Andrade JM, **Shiozawa Y**, **Peters C**. Characterization of a syngeneic mouse model of prostate cancer induced bone pain. Neuroscience 2019, Chicago, IL, USA, October 19-23, 2019. Poster.

Website(s) or other Internet site(s)

Nothing to report.

Technologies or techniques

Nothing to report.

Inventions, patent applications, and/or licenses

Nothing to report.

Other products

Nothing to report.

7. PARTICIPANTS & OTHER COLLABORATING ORGANIZATIONS

What individuals have worked on the project?

Name: Yusuke Shiozawa
Project Role: PI, W81XWH-17-1-0541
Researcher Identifier (e.g. ORCID ID): orcid.org/0000-0001-9814-9230
Nearest person month worked: 3
Contribution to Project: Dr. Shiozawa is an Assistant Professor in the Department of Cancer Biology. He has extensive experience in the study of prostate cancer bone metastasis, and will provide oversight of the entire program including development and implementation of all policies, procedures, and processes. In this role, Dr. Shiozawa will be responsible for the completion of the project and for ensuring that systems are in place to guarantee institutional compliance with US laws, including biosafety and animal research guidelines, data collection and analyses, and facilities. Dr. Shiozawa will supervise other personnel on the project to ensure timely and effective studies.
Funding Support: Department of Defense, TEVA Pharmaceuticals

Name: Christopher Peters
Project Role: Partnering PI, W81XWH-17-1-0542
Researcher Identifier (e.g. ORCID ID):
Nearest person month worked: 1.8
Contribution to Project: Dr. Peters is an Assistant Professor in the Department of Anesthesiology. Dr. Peters' research interests are in central and peripheral mechanisms of pain chronicity including postsurgical, bone cancer and chemotherapy induced pain and neuropathy. Dr. Peters will be responsible for supervising and training personnel in evoked and non-evoked bone cancer pain behavioral assays. As part of Aims 1 and 3, Dr. Peters will assist with *in vivo* validation of a viral vector approach for sensory neuron selective knockdown of ATR and CGRP. He will also assist with histological and immunohistochemical analysis of skeletal tissue as part of Aims 1-3. Dr. Peters has over 15 years of experience working with preclinical models of skeletal pain including rat and mouse models of bone cancer. He has extensive experience with the behavioral analysis, immunohistochemistry, biochemical analysis and fluorescent, brightfield, and confocal microscopic imaging required for this project. He will meet with Dr. Shiozawa on a weekly basis to discuss progress on projects related to this Partnering PI Prostate Cancer Research Idea Development Award.
Funding Support: National Institutes of Health, Department of Defense

Name: Fang-Chi Hsu
Project Role: Co-Investigator, W81XWH-17-1-0541
Researcher Identifier (e.g. ORCID ID):
Nearest person month worked: 0.6
Contribution to Project: Dr. Hsu is a Professor in the Department of Biostatistical Sciences. She will work closely with Dr. Shiozawa and the team to analyze the results of the project.
Funding Support: National Institutes of Health, Department of Defense

Name: Christopher Thomas
Project Role: Co-Investigator, W81XWH-17-1-0541
Researcher Identifier (e.g. ORCID ID):
Nearest person month worked: 0.12

Contribution to Project: Dr. Thomas is an Associate Professor in the Department of Hematology/Oncology. On this project, he will assist Dr. Shiozawa's laboratory in tissue procurement, experimental design, and scientific strategy.
Funding Support: Department of Defense

Name: Debra Diz
Project Role: Co-Investigator, W81XWH-17-1-0541
Researcher Identifier (e.g. ORCID ID):
Nearest person month worked: 0.6
Contribution to Project: Dr. Diz is the Co-Director of the Cardiovascular Sciences Center and Professor, Department of General Surgery. Her research focuses on cardiovascular neuroscience and neuropharmacology related to the effects of angiotensin II on neuropeptide and release of other transmitters in the context of the renin-angiotensin-system in aging and metabolic regulation. On this project, she will assist Dr. Shiozawa's laboratory in radio binding assay.
Funding Support: National Institutes of Health, Department of Defense

Name: Mark Chappell
Project Role: Co-Investigator, W81XWH-17-1-0541
Researcher Identifier (e.g. ORCID ID):
Nearest person month worked: 0.6
Contribution to Project: Dr. Chappell is a Professor in the Department of General Surgery and member of the Cardiovascular Sciences Center. He is an expert in the assessment of the renin-angiotensin-system (RAS) components and is interested in the RAS in hypertension, diabetes, fetal programming and women's health issues. On this project, he will assist Dr. Shiozawa's laboratory in radioimmnunoassay.
Funding Support: National Institutes of Health, Department of Defense

Name: Thomas Jeff Martin
Project Role: Co-Investigator, W81XWH-17-1-0542
Researcher Identifier (e.g. ORCID ID):
Nearest person month worked: 0.6
Contribution to Project: Dr. Martin is a Professor in the Department of Anesthesiology and Physiology & Pharmacology. Dr. Martin's research interests are on mechanisms of opioid abuse particularly in the setting of chronic pain. He has been instrumental in the development of operant based behavioral assays to monitor the effects of persistent pain on complex animal behaviors. Dr. Martin will assist with training, implementation and analysis of running wheel assays to assess progressive disability in mice inoculated with bone cancer as part of studies outlined in Aims 1-3.
Funding Support: National Institutes of Health, Department of Defense

Name: Juan Miguel Jimenez-Andrade
Project Role: Visiting scholar, W81XWH-17-1-0542
Researcher Identifier (e.g. ORCID ID):
Nearest person month worked: 3
Contribution to Project: Dr. Jimenez-Andrade is a Professor in the Autonomous University of Tamaulipas in Reynosa, Mexico. Dr. Jimenez-Andrade's laboratory research is focused on mechanisms of skeletal pain and osteoporosis. He assumed responsibility for performing microCT imaging and analysis as part of experiments in Aims 1-3. The subaward initially established with Ted Bateman at UNC was transferred to Dr. Jimenez-

Andrade's institution effective September 2019. Additionally, he will assist with immunohistochemical analysis of decalcified bone sections as part of studies under this proposal.
Funding Support: Department of Defense, National Institutes of Health, UC MEXUS-CONACYT

Has there been a change in the other active support of the PD/PI(s) or senior/key personnel since the last reporting period?

Nothing to report.

What other organizations have been involved as partners?

The Autonomous University of Tamaulipas at Reynosa Mexico

8. SPECIAL REPORTING REQUIREMENTS:

QUAD CHARTS.

9. APPENDICES:

The original copies of manuscript are attached.

Molecular crosstalk: bone metastatic prostate cancer and nociceptive neurons

PC160455, PC160455P1

W81XWH-17-1-0541, W81XWH-17-1-0542

PI: Yusuke Shiozawa, Christopher Peters **Org: Wake Forest University Health Sciences** **Award Amount:** $500,001 (Shiozawa)
$496,403 (Peters)

Study/Product Aim(s)

- **Aim 1: Determine how disseminated prostate cancer is involved in development of cancer-induced bone pain.**
- **Aim 2: Define the intracellular signaling pathways in peripheral nerves stimulated by disseminated prostate cancer.**
- **Aim 3: Determine the influence of nociceptive neurons on (a) tumor outgrowth in the bone and (b) cancer-induced bone pain.**

Approach

The goal of this project is to determine the roles of the interaction between bone metastatic prostate cancer and sensory nerves in cancer-induced bone pain and bone metastatic growth using our innovative mouse models that enable us to measure cancer bone pain, tumor growth, and bone dynamics within the same animals. In addition, using biopsy samples from patients, we will verify the results from the animal experiments.

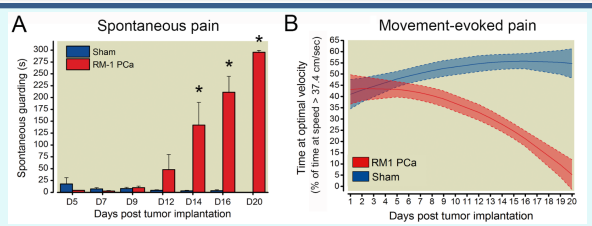

Assessment of pain behaviors of mice inoculated into femur with PCa cells. Time course of ongoing or spontaneous pain in mice following intra-femoral-injection of RM-1 PCa cells or sham injections is evident as progressive increase in duration of guarding of the tumor bearing hindlimb (A). Two-way RM ANOVA with Bonferroni comparisons *P<0.05 versus sham values within time point. Sham n=8, RM-1 n=9. Tumor bearing mice also displayed progressive impairment in the time spent running at an optimal velocity during daily 30 minute sessions compared to sham mice (B) potentially reflecting movement evoked pain or cancer induced functional disability. Longitudinal running wheel data best fit a quadratic form. Mice inoculated with RM-1 demonstrated a significantly decelerating trajectories (Time^2 X Group, p= 0.003) but similar intercepts (Group, p= 0.65). Sham n= 12, RM-1 n=12.

- We developed a syngeneic mouse bone metastatic model which allows us to measure progressive bone pain behaviors.

Timeline and Cost

Activities CY	17	18	19	20
Aim 1 (Animal Studies)				
Aim 2 (Animal Studies)				
Aim 2 (Bone sample analyses)				
Aim 3 (Animal Studies)				
Estimated Budget ($K)	**$100**	**$325**	**$325**	**$246**

Updated: 10/18/2018

Goals/Milestones (Example)

CY17 Goal – Team development

☑ Set up and organize the monthly meeting

CY18 Goals – Animal studies

☑ Develop the technique to manipulate gene in nerves with vector

☑ Determine the roles of nerves in cancer progression

CY19 Goal – Bone biopsy sample analyses/Animal studies

☑ Develop the system to assess bone biopsy samples

☑ Determine the roles of nerves in cancer progression

☑ Determine the roles of cancer in cancer-induced bone pain

CY20 Goal – Bone biopsy sample analyses/Animal studies

☐ Determine the roles of cancer in cancer-induced bone pain

☐ Assess the nerve/cancer interaction in bone biopsy samples

Comments/Challenges/Issues/Concerns

- Nothing to report.

Budget Expenditure to Date

Projected Expenditure: $750K

Actual Expenditure: $667K

NEOPLASIA
www.neoplasia.com

Volume 21 Number 2 February 2019 pp. 172–184 172

Trabectedin Reduces Skeletal Prostate Cancer Tumor Size in Association with Effects on M2 Macrophages and Efferocytosis[1,2]

J.D. Jones[*,3], B.P. Sinder[*,3], D. Paige[*], F.N. Soki[*], A.J. Koh[*], S. Thiele[†,‡], Y. Shiozawa[*,§], L.C. Hofbauer[†,‡], S. Daignault[¶], H. Roca[*] and L.K. McCauley[*,#]

[*]Department of Periodontics and Oral Medicine, University of Michigan School of Dentistry, Ann Arbor, MI; [†]Department of Endocrinology, Diabetes, and Bone Disease, Technische Universität Dresden Medical Center, Dresden, Germany; [‡]German Cancer Consortium (DKTK), partner site Dresden and German Cancer Research Center (DKFZ), Heidelberg, Germany; [§]Department of Cancer Biology and Comprehensive Cancer Center, Wake Forest University School of Medicine, Winston-Salem, NC; [¶]Department of Biostatistics, Center for Cancer Biostatistics, University of Michigan, Ann Arbor, MI; [#]Department of Pathology, University of Michigan Medical School, Ann Arbor, MI

Abstract

Macrophages play a dual role in regulating tumor progression. They can either reduce tumor growth by secreting antitumorigenic factors or promote tumor progression by secreting a variety of soluble factors. The purpose of this study was to define the monocyte/macrophage population prevalent in skeletal tumors, explore a mechanism employed in supporting prostate cancer (PCa) skeletal metastasis, and examine a novel therapeutic target. Phagocytic CD68+ cells were found to correlate with Gleason score in human PCa samples, and M2-like macrophages ($F4/80^+CD206^+$) were identified in PCa bone resident tumors in mice. Induced M2-like macrophages *in vitro* were more proficient at phagocytosis (efferocytosis) of apoptotic tumor cells than M1-like macrophages. Moreover, soluble factors released from efferocytic versus nonefferocytic macrophages increased PC-3 prostate cancer cell numbers *in vitro*. Trabectedin exposure reduced M2-like (F4/80+CD206+) macrophages *in vivo.* Trabectedin administration after PC-3 cell intracardiac inoculation reduced skeletal metastatic tumor growth. Preventative pretreatment with trabectedin 7 days prior to PC-3 cell injection resulted in reduced M2-like macrophages in the marrow and reduced skeletal tumor size. Together, these findings suggest that M2-like monocytes and macrophages promote PCa skeletal metastasis and that trabectedin represents a candidate therapeutic target.

Neoplasia (2019) 21, 172–184

Abbreviation: PCa, Prostate Cancer.

Address all correspondence to: Laurie K. McCauley, Department of Periodontics and Oral Medicine, University of Michigan School of Dentistry, 1101 N. University Avenue, Ann Arbor, MI 48109-1078. E-mail: mccauley@umich.edu

[1] Financial Support: This work was supported by the Department of Defense (W81XWH-14-1-0408) to Jacqueline D. Jones and Benjamin P. Sinder; Department of Defense Physician Research Training Award (W81XWH-14-1-0287) and PCF Young Investigator Award to Todd M. Morgan; Department of Defense (W81XWH-14-1-0403 and W81XWH-17-1-0541 (Y.S.)) to Yusuke Shiozawa; NIH: National Cancer Institute PO1CA093900 to Laurie K. McCauley, Yusuke Shiozawa, NIH: National Cancer Institute F32 CA168269 to Fabiana N. Soki; and Deutsche Forschungsgemeinschaft (Forschergruppe-1586 SKELMET and SPP-2084 μBONE) to S. Thiele and Lorenz C. Hofbauer.
[2] Disclosure and Conflict of Interest: L. C. H.: consultancy for Alexion, Amgen, Sandoz, Shire, Radius, and UCB.All others: no potential conflicts of interest are disclosed.
[3] Denotes co-first authors.
Received 3 April 2018; Revised 7 November 2018; Accepted 9 November 2018

1476-5586
https://doi.org/10.1016/j.neo.2018.11.003

Introduction

Bone marrow is the preferred metastatic site for prostate cancer and is rich in monocytic cells [1]. Cells of the myeloid lineage have been implicated as tumor-associated macrophages and myeloid-derived suppressor cells in the pathophysiology of various cancers [2,3]. Patients with prostate cancer (PCa) skeletal metastasis experience severe morbidity and mortality, and while macrophage targeting strategies could yield more effective therapeutic options, relatively little is known about monocytic cells in the pathophysiology of skeletal metastasis.

Monocytes and macrophages are highly heterogeneous populations with diverse subpopulations that have distinct phenotypes. A convenient paradigm for classifying macrophages is into proinflammatory "classically activated" M1-like and anti-inflammatory "alternatively activated" M2-like macrophage subtypes. Interestingly, M2-like $CD14^+CD16^+$ monocytes are elevated in the blood of cholangiocarcinoma patients, correlate with tumor-associated macrophage infiltration [4], and associate with tumor progression [4–7].

A key macrophage function is efferocytosis (phagocytosis of apoptotic cells), and macrophages are literally named for their phagocytic nature. M2-like macrophages have been positively associated with efferocytic capacity. Moreover, macrophage efferocytosis is known to induce secretion of key factors that have been implicated in tumor progression including TGF-β and CCL2 [8–10]. Indeed, previous work has demonstrated that compromised macrophage efferocytosis in MFG-E8 KO mice results in both reduced M2 polarization and prostate cancer tumor growth [9]. Therapeutic strategies to inhibit monocytes, M2-like macrophages, and efferocytosis could prove particularly beneficial to skeletal metastatic outcomes.

To explore the role of macrophages in prostate cancer skeletal metastasis and a novel treatment strategy, this study utilized the FDA-approved chemotherapeutic trabectedin (ecteinascidin 743). While trabectedin can directly inhibit certain types of cancer cells, it was recently identified to also have a highly selective and proficient ability to induce apoptosis in monocytes and macrophages [11]. In fact, trabectedin significantly reduced tumor size in cancer cells resistant to trabectedin treatment, suggesting that macrophage effects were important to its therapeutic benefit [11]. Although this demonstrated the importance of trabectedin's macrophage targeting effects, it focused solely on subcutaneous models of primary fibrosarcomas.

Given that bone marrow is the preferred metastatic site for PCa and has a unique cellular microenvironment rich in many cell types including monocytes, the present study investigated the macrophage subtypes and new treatment strategies for PCa skeletal metastasis. Specifically, two treatment strategies were explored: 1) a "preventative" treatment whereby trabectedin was administered before tumor cell inoculation to determine the impact of modulating macrophages in the bone marrow microenvironment and their role in tumor colonization of the bone microenvironment and 2) a "therapeutic" treatment regimen where trabectedin was administered after intracardiac injection of prostate cancer cells to reduce metastasis.

Materials and Methods

Cells

Luciferase-labeled PC-3 cells ($PC\text{-}3^{Luc}$) were established from the PC-3 cell line (American Type Culture Collection) as previously described [12]. $PC\text{-}3^{Luc}$ cells were regularly authenticated and matched short tandem repeat DNA profiles of the original PC-3 cell line (IDEXX Bioresearch, Westbrook, ME). Bone marrow macrophages were collected from C57BL/6J mice (Jackson laboratory, Bar Harbor) at 4-6 weeks of age for *ex vivo* and *in vitro* experiments. For *in vitro* experiments, macrophages were differentiated from bone marrow using α-MEM media with 30 ng/ml murine macrophage-colony stimulating factor (M-CSF) (eBioscience) for 6 days. At day 7, macrophages were collected and used for further analyses. For macrophage polarization, cells were treated with either IL-4 (R&D Systems) (alternatively activated-M2) or IFNγ (R&D Systems) (classically activated-M1) for 24 hours prior to efferocytosis and flow cytometric analyses. Apoptosis of PCa cells was induced by UV radiation treatment for 30 minutes followed by a 1-hour incubation at 37°C with 5% CO_2. Cells were considered highly apoptotic (HAp) if there were 70% or higher trypan blue–positive cells. Untreated tumor cells with <10% trypan blue–positive cells were considered basal apoptotic cells (BAp) as previously described [9]. Osteoclastogenesis was induced as previously described [13]. Briefly, freshly isolated bone marrow cells were treated with 30 ng/ml M-CSF and 50 ng/ml RANKL (R&D Systems). Medium was changed every 2 days. At day 7, cells were treated with or without trabectedin for 24 hours and subsequently stained for tartrate resistant acid phosphatase (TRAP) activity.

Drug

Trabectedin (PharmaMar, Colmenar Viejo, Madrid Spain) was dissolved in dimethylsulfoxide. For *in vitro* experiments, cells were treated with trabectedin (10 nM) for 24 hours. For *in vivo* experiments, mice were administered trabectedin (0.15 mg/kg/bodyweight) intravenously via tail vein injection as described [11].

Efferocytosis Assays

Bone marrow macrophages were stained with Cell Trace CSFE (Invitrogen) at 0.2 μl/ml. Fluorescently stained bone marrow cells were then co-cultured with phosphatidylserine (PS)-coated (Abcam) fluorescently labeled apoptotic mimicry beads (Bangs Laboratories, Inc.) or fluorescently tagged apoptotic PC-3 cells at a 1:3 ratio of macrophages to apoptotic bait at 37°C. Cells were washed with PBS, fixed with 10% formalin, and collected for further analysis.

Flow Cytometry

Cells (1×10^6) were resuspended in FACS buffer (PBS, 2% FBS, and 2 mM EDTA) for antibody exposure. Fluorochrome-labeled antibodies against monocyte and macrophage specific markers including F4/80 (Abcam C1:A3-1), CD86 (BioLegend GL-1), CD206 (BioLegend C068C2), CD68 (BioLegend FA-11), CD45 (BioLegend 30-F11), CD115 (BioLegend AFS98), and tumor necrosis factor receptor superfamily, member 10b (TRAILR2) (R&D Systems FAB721C) were added for 30 minutes on ice and washed three times with cold PBS. Controls included unstained samples for cell size assessment and isotype IgG control (BD Pharmingen) tagged antibodies. After antibody incubation, cells were washed twice with FACS buffer and fixed with 1% formalin. For intracellular staining, cells were subsequently permeabilized with Leucoperm (AbD Serotec) and incubated with antibodies. Data were collected and evaluated for flow cytometry analyses using BD FACSAria III and FlowJo v10 software.

RNA Extraction and Quantitative PCR

RNA isolation was performed as described previously [14] using an RNeasy mini kit (Qiagen, Valencia, CA). The cDNA

was synthesized using 0.5μg of total RNA in 50 μl of reaction volume using the TaqMan reverse transcription kit (Applied Biosystems). Quantitative real-time PCR was performed with ABI PRISM 7700 using a ready-to-use mix of primers and FAM labeled probe assay systems (Applied Biosystems) for transforming growth factor beta-1 or *Tgf-β1* (*Tgfb1*, Mm03024053_m1), chitinase-like 3 or Ym1 (*Chi3l3*, Mm00657889_mH), and tumor necrosis factor alpha-like or TNF-α (*Tnf*, Mm00443260-g1). GAPDH (*Gapdh*, Mm99999915_g1) was used as an endogenous control, and the ΔΔCT method was used to calculate the data as described previously [15].

Western Blot Analyses and Quantification

Western blot analysis and quantification were performed as previously described [9]. Primary antibodies against β-actin (1:5000, Abcam, 8227), colony stimulating factor 1 receptor (CD115) (1:1000, Abcam, 74121), and TRAILR2 (1:1000, Abcam, 8416) were used. Protein quantification was performed using the Scion Image software and calculated relative to control protein expression (β-actin).

Transwell Chemotaxis Assay for Cell Proliferation

PC-3^{Luc} cells were seeded (2.0×10^4 cells/well) onto 6-well culture plates. M-CSF expanded bone marrow–derived macrophages were loaded (1:3) into top cell culture 0.4-μm Transwell inserts (EMD Millipore) alone or with UV-induced apoptotic PC-3^{Luc} cells on day 0 and again on day 4. To measure tumor cell growth, Transwell inserts were removed, and tumor cell growth was measured using bioluminescence.

Murine Tumor Models

All animal experiments were executed under the approval and guidance of the Institutional Animal Care and Use Committees of the University of Michigan. Male athymic mice were obtained from Harlan Laboratories (Haslett, MI). For the orthotopic bone tumor model, 1×10^3 PC-3^{Luc} cells were injected into both proximal tibiae of 4- to 6-week-old athymic male mice as previously described [16]. For the experimental skeletal metastasis model, 2×10^5 PC-3^{Luc} cells were injected into the left ventricle of the heart of male athymic mice [16]. To monitor tumor growth, mice were imaged weekly via bioluminescence. After 6 weeks, animals were sacrificed and hind limbs were collected for further analysis.

Histology and Staining

After euthanasia, hind limbs were harvested and fixed with 4% paraformaldehyde/PBS at 4°C for 24 hours. Bones were then decalcified in 10% EDTA for 2 weeks and embedded in paraffin. Immunohistochemical staining was performed using a cell and tissue staining assay (HRPDAB system; R&D systems) with rabbit polyclonal antibody to CD206 (1:100; Abcam) and mouse monoclonal antibody to CD68 (1:100; Abcam). Negative controls were used to detect nonspecific staining. TRAP staining on bone sections was performed using a TRAP staining kit (Sigma-Aldrich) according to manufacturer's instructions. Staining was quantified by counting three different fields of view per specimen at 400× magnification that representatively sampled the tumor in the bone marrow. On H&E-stained sections from midtibia, bone area per tissue area was quantified in Osteomeasure software. Tissue area spanned the endocortical border and began 0.3 mm from the growth plate and extended 1 mm distally.

A human prostate cancer tissue microarray was stained for CD68 (KP1, 1:200). A representative subset of 46 patients was analyzed from a TMA containing >400 patients as previously published [17]. Assessment was carried out by one/two independent investigator/s that was/were blinded to the clinical information. The 46 patient cohort consisted of 16 benign prostatic hyperplasia (BPH), 22 Gleason ≤ 7, and 36 Gleason ≥ 8 patients. Staining was quantified by counting the sum of four different fields of view for positively stained cells at 200× magnification per specimen.

Inflammatory Cytokine Array

Serum from trabectedin-treated and control mice was collected at the end of the 6-week study. Cytokines were analyzed using the mouse inflammation antibody array C1 according to the manufacturer's instructions (AAM-INF-1-8, RayBiotech, Inc.).

Figure 1. Phagocytic CD68+ cells are positively associated with high Gleason scores, and macrophage efferocytosis supports prostate cancer cell growth. (A) Representative images of CD68 immunohistochemistry in prostate cancer tissue microarray specimens including BPH ($n=16$), Gleason ≤7 ($n=22$), and Gleason ≥8 ($n=36$). Arrowheads (black) indicate cells positive for CD68. Images are taken at 400-fold magnification. (B) Quantitative analysis of tissue specimens for the sum of CD68$^+$ cells in four different fields of view. Measured images were taken at 20× for analysis. Data are mean ± SE, *P<.05, **P<.01. (C) The association of two or more CD68$^+$ cells in tissue by patient's Gleason score was tested using Fisher's exact test. Significance was set at *P<.05. (D-E) Murine bone marrow–derived macrophages were cultured with PS-coated apoptotic mimicry beads (3:1) or fluorescently labeled apoptotic PC-3 cells (2:1) *ex vivo*, and efferocytosis was analyzed using flow cytometry for ingested beads/cells. (D) PE-labeled and unlabeled PS-coated apoptotic mimicry beads were cultured with freshly isolated bone marrow cells and analyzed by flow cytometry for F4/80$^+$ cells with ingested beads. Data are mean ± SE ($n=4$/group), *P<.05. (E) UV-induced apoptotic prostate cancer PC-3 cells (>60% high apoptosis, HAp) or noninduced PC-3 cells (<10% basal apoptosis, BAp) were cultured with freshly isolated bone marrow cells and analyzed by flow cytometry for F4/80$^+$ cells with ingested PE-labeled apoptotic tumor cells. Representative images shown with data indicated at upper right as mean ± SE ($n=4$/group), P<.05. (F-I) Pretreatment with IL4 and IFN-γ induced polarization into M1 or M2-like macrophages. (F,G) Cell surface markers F4/80, CD86, and CD206 were used to identify polarized macrophage populations using flow cytometry. Percent (%) parent population indicates the number of positive cells in the percentage of total cell population. Data are mean ± SE ($n=4$/group), #P<.0001. Representative flow cytometry images are below. (H) Relative gene expression of YM1, TGF-β, and TNF-α in polarized macrophages. Data are mean ± SE ($n=4$/group), *P<.05 vs. control. (I) Macrophage efferocytosis using fluorescently labeled HAp (PC-3) tumor cells as bait to determine the preferential behavior of polarized M1 (IFN-γ) versus M2 (IL-4) macrophages. Data are mean ± SE ($n=4$/group), *P<.05. (J) Schematic representation of experimental design to evaluate the effect of macrophages on PC-3 cell proliferation. (K) PC-3^{Luc} cells as shown in F were used to measure cell growth as a result of macrophage efferocytosis using a Transwell assay. Data are mean ± SE ($n=3$/group), *P<.05 vs. all other groups.

Statistical Analyses

Continuous outcomes are reported using means and standard errors by group. Student's *t* test was used for testing differences between two groups. Two-way ANOVA was used for two-factor experiments. Proportions of patients with two or more $CD68^+$ cells by Gleason sum were compared using Fisher's exact test. GraphPad Prism and SAS 9.3 were used for statistical analysis with a significance threshold of $P<.05$.

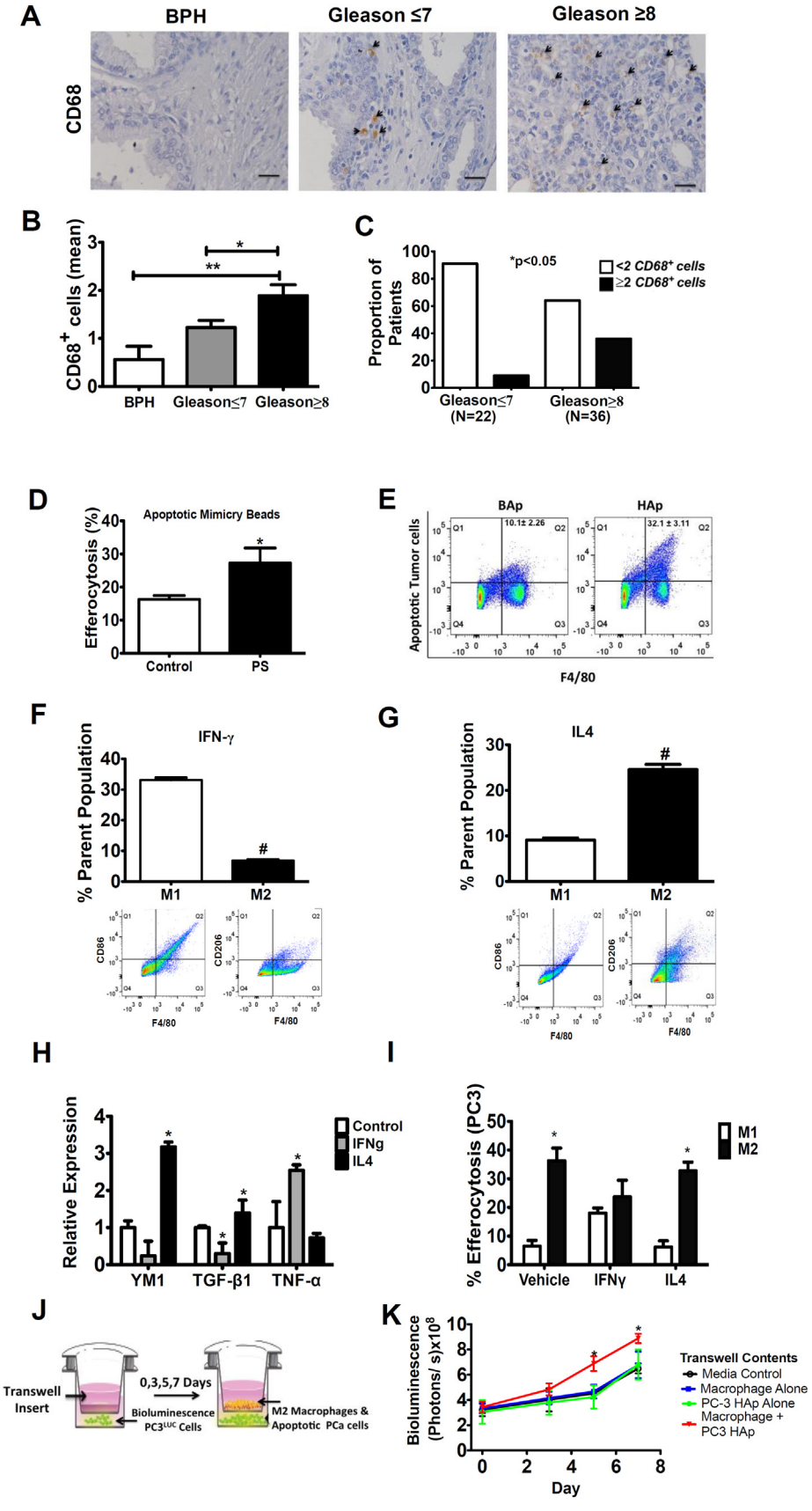

Results

Phagocytic CD68+ Cells Positively Associated with High Gleason Scores

Human prostate cancer tissue samples were first evaluated to determine the association of macrophages in the pathophysiology of prostate cancer and their potential as therapeutic targets. Monocytes were stained for CD68 expression, a scavenger receptor with an established role in phagocytosis. Samples were taken from patients characterized by BPH (n=16), Gleason score of ≤7 (n=22), and a Gleason score of ≥8 (n=36) (Figure 1*A*). Little to no expression of $CD68^+$ cells was identified in BPH specimens. Increasing numbers of CD68-positive macrophages were identified with the higher grade. Quantitative analysis of the tissue microarray revealed significantly increased numbers of $CD68^+$ cells in high-risk patients with a Gleason score ≥8 (Figure 1*B*). Further, patients with Gleason score ≥8 were more likely to have two or more $CD68^+$ cells identified compared to patients with a Gleason score ≤7 (Figure 1*C*). These data demonstrate a positive association of CD68 staining with higher-risk patients and support further exploration of macrophage and phagocytic therapeutic targets.

Prostate Cancer Cell Growth Enhanced with Macrophage Efferocytosis

The role of macrophage efferocytosis in prostate cancer cell growth was first examined with freshly isolated bone marrow cells using two different bait models (apoptotic cells or beads phagocytosed by macrophages) and analyzed using flow cytometry. Murine F4/80–positive bone marrow macrophages cultured with phosphatidylserine coated apoptotic mimicry beads displayed a significantly higher percentage of efferocytosis compared to uncoated beads (Figure 1*D*). Similarly, efferocytosis was significantly enhanced when induced highly apoptotic (HAp) PC-3 cells were incubated with F4/80 marrow macrophages compared to noninduced basal apoptotic (BAp) PC-3 cells (32.1% ± 3.1 vs. 10.1% ± 2.3) (Figure 1*E*).

Enhanced efferocytosis has been associated with cytokines that induce macrophage polarization such as IL-4 [18]. M-CSF expanded bone marrow–derived macrophages were treated with IFN-γ to induce polarization to an M1-like phenotype ($F4/80^+$, $CD86^+$), or IL-4 for an M2-like phenotype ($F4/80^+$, $CD206^+$) (Figure 1, *F*, *G*). Gene expression of TNF-α, a proinflammatory marker, was significantly increased in IFN-γ polarized macrophages. Conversely, genes associated with an anti-inflammatory response, including Ym1 and TGFβ [19,20], were significantly higher in the IL-4 polarized macrophages (Figure 1*H*).

To evaluate whether M1 or M2 macrophages are more adept at efferocytosis, HAp PC-3 cells were cultured with M1 or M2 bone marrow–derived macrophages. M2 macrophages were more proficient at efferocytosis than M1 macrophages (Figure 1*I*). Next, to evaluate the impact of efferocytosis on prostate cancer proliferation, luciferase-labeled tumor cells were incubated in a Transwell assay with macrophages undergoing efferocytosis or control macrophages as depicted in Figure 1*J*. When HAp PC3 cells were used as bait, significantly increased tumor cell growth was observed compared to all control groups (Figure 1*K*). Interestingly, the presence of macrophages alone was not sufficient to induce significant growth of tumor cells (Figure 1*K*), suggesting that the efferocytic function was required.

Single Administration of Trabectedin Reduced M2-Like Macrophages

Given the effect of M2 macrophages on efferocytosis *in vitro*, the impact of the macrophage-targeting agent trabectedin was first evaluated in the bone marrow metastatic environment without the confounding impact of a tumor as depicted in Figure 2*A*. Mice were analyzed 7 days posttreatment to ensure that the drug was completely cleared before analyzing the bone marrow and blood cellular profiles [21,22]. Trabectedin-treated mice had significantly reduced circulating $CD115^+$ blood mononuclear cells, while no significant differences were found in $CD11b^+$ or $CD45^+$ cells alone and in combination compared to vehicle control mice (Figure 2*B*). In the bone marrow microenvironment, trabectedin significantly reduced $F4/80^+$, M2-like cells ($F4/80^+$/$CD206^+$) but not M1-like cells ($F4/80^+$/$CD86^+$) (Figure 2*C*). These data suggest that M2-like cells ($F4/80^+$/$CD206^+$) macrophages and $CD115^+$ mononuclear cells are more susceptible to trabectedin treatment.

"Preventative" Trabectedin Treatment Regimen Reduces M2-Like Macrophages and Skeletal Tumor Size

Bone marrow has a high cell turnover rate, which suggests the need for phagocytic cells to engage in rapid clearance of apoptotic cells, and the presence of tumor cells in the bone can further increase the need for efferocytosis. Current work has shown that M2 polarization can be a contributing factor to tumor growth due to the release of protumorigenic factors like TGF-β, and M2-like macrophage density has been linked with tumor progression [23]. However, a defined monocyte and macrophage population in the context of PCa resident in the bone has not been fully delineated. The effect of monocyte and macrophage targeting via trabectedin was determined in an orthotopic bone prostate tumor mouse model (Figure 3*A*). A single administration of trabectedin 7 days prior to tumor inoculation resulted in decreased tumor bioluminescence in the tibiae as early as day 28 (Figure 3*B*). The mice were sacrificed at day 42 and the circulating monocytes and bone marrow cells were analyzed. Mice bearing tumors and treated with trabectedin for 6 weeks showed no differences in $CD45^+$ cells but had a trend toward an overall increase in $CD115^+$ (P=.064) cells and a significant increase in $CD11b^+$ cells (Figure 3*C*). Interestingly, in the trabectedin-treated bone marrow of resident tumor cells, a significant decrease was seen in $F4/80^+$, $CD206^+$, and $F4/80^+$/$CD206^+$ double-positive cells (Figure 3*D*). There were no differences in $CD86^+$ cells and the M1 population ($F4/80^+CD86^+$ double-positive cells) between vehicle- and trabectedin-treated mice (Figure 3*D*). The amount of bone in the tibia relative to the tissue area was not significantly different with trabectedin treatment (Suppl. Figure 3*A*). Collectively, these data show that mice treated with a single administration of trabectedin exhibited a sustained decrease in M2-like macrophages, and despite the increase in circulating $CD11b^+$ cells, this resulted in decreased tumor burden.

Reduced M2-Like Macrophages in Trabectedin-Treated, Prostate Tumor–Bearing Mice

As CD115 has been shown to be associated with resident macrophages and mature monocytes [24], the effects of trabectedin on tumor-bearing hind limbs (tibiae) were analyzed via immunohistochemistry. $CD68^+$ cells were concentrated in areas in close proximity to tumors, whereas, in trabectedin-treated mice, $CD68^+$ cell density was reduced and scattered throughout the tissue (Figure 4*A*). Although differences in $CD68^+$ cells were not identified by flow cytometric analysis of the tibia, immunohistochemistry analysis revealed a significant reduction in $CD68^+$ cells in the tissue (Figure 4*B*). $CD206^+$ cells were present in both treated and

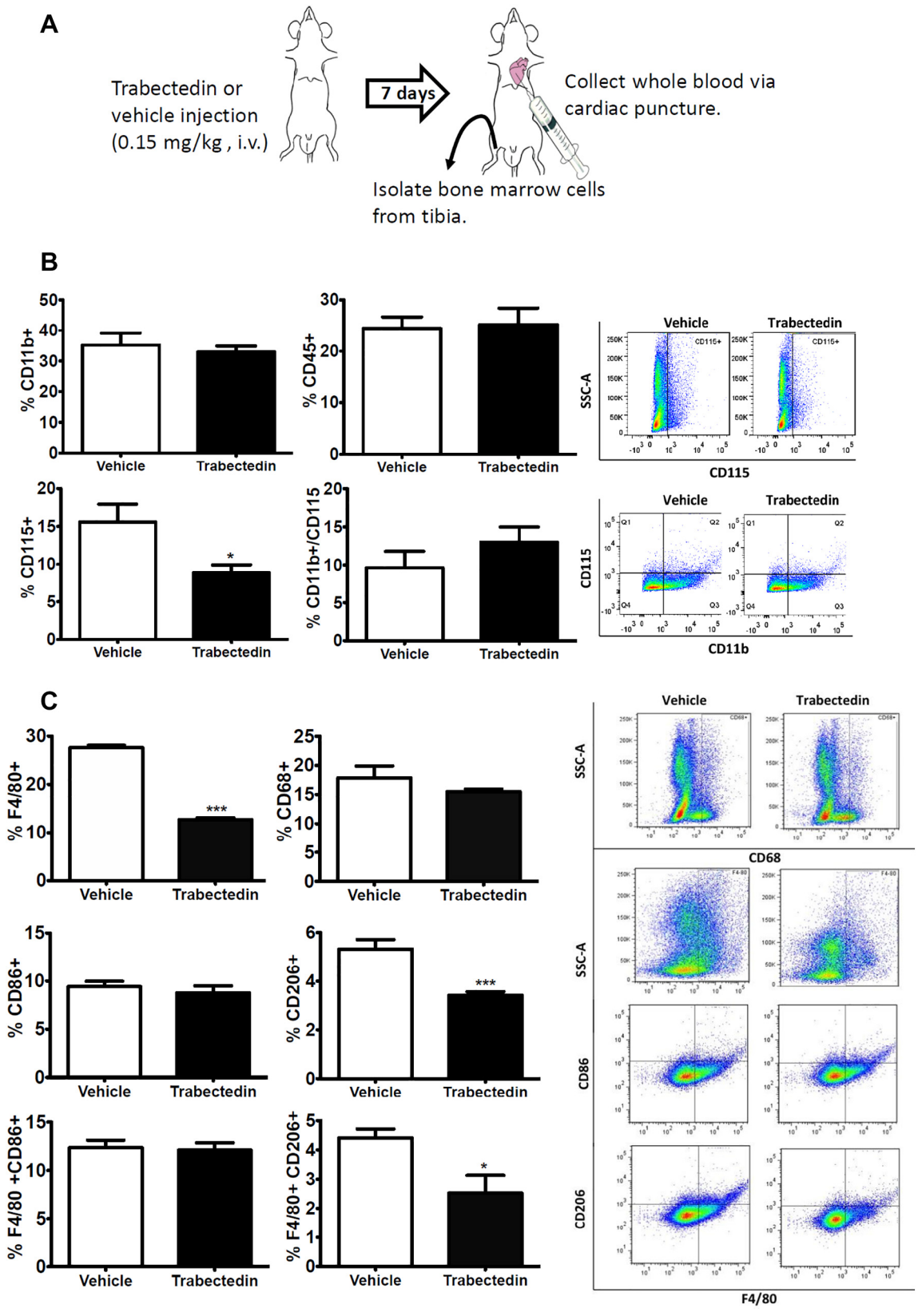

Figure 2. Single dose of trabectedin significantly reduces M2-like bone marrow cells *in vivo*. (A) Schematic representation of the experimental design. Male athymic mice were divided into two groups and treated with a single intravenous injection of saline or trabectedin (0.15 kg/mg/bodyweight). Seven days postadministration, whole blood and bone marrow cells were collected. (B) Monocytes were isolated from whole blood and flow cytometric analyses performed for $CD11b^+$, $CD45^+$, and $CD115^+$ cells. Representative flow cytometric analyses are shown. Data are mean ± SE (n=5/group), *P<.05 vs. vehicle. (C) Bone marrow cells were isolated and analyzed for markers F4/80, CD68, CD86, and CD206 using flow cytometric analyses. Representative flow cytometric analyses are shown. Data are mean ± SE (n=5/group), *P<.05, ***P<.001 vs. vehicle.

untreated mice; however, like CD68$^+$ cells in the tissue, CD206$^+$ cells appeared more dispersed throughout the tissue in treated mice (Figure 4*C*). Quantitative analysis of CD206$^+$ cells in four different areas per tibiae revealed a significant decrease in trabectedin-treated mice (Figure 4*D*). Since monocytes serve as progenitors to osteoclasts, osteoclast numbers were analyzed. Representative images of osteoclasts in the bone of tumor-bearing mice treated or untreated with trabectedin are shown in Figure 4*E*. Quantitative analysis of the number of osteoclasts was not significantly different in trabectedin-treated versus untreated mice (Figure 4*F*). These data suggest that trabectedin preferentially targeted phagocytic CD68$^+$ and CD206$^+$ cells but did not significantly decrease osteoclast number.

"Therapeutic" Trabectedin Treatment Regimen Reduces M2-Like Macrophages and Skeletal Metastasis

To investigate the effect of circulating monocytes in prostate cancer skeletal metastasis, an intracardiac skeletal metastatic tumor model for prostate cancer was utilized (Figure 5*A*) [25]. Trabectedin-treated mice presented a significant decrease in tumor bioluminescence in the hind limbs at day 35 vs. vehicle controls (Figure 5, *B-C*). Tumor bioluminescence in the mandible was significantly decreased only at day 42 (Figure 5, *B* and *D*). Interestingly, a significant decrease in F4/80$^+$, CD68$^+$, CD206$^+$, and double-positive F4/80$^+$/CD86$^+$, F4/80$^+$/CD206$^+$ cells were identified in the tibiae of trabectedin-treated mice at the end of 6 weeks (Figure 5*E*). CD11b+ cells in the blood were increased with trabectedin treatment (Suppl. Figure 2). Bone area per tissue area was reduced with trabectedin treatment (Suppl. Figure 3*B*). Trabectedin-treated mice showed a significant increase in proinflammatory cytokine levels of IL-12 ($P<.03$); soluble tumor necrosis factor receptor superfamily, member 1A (sTNFR1) ($P<.04$); chemokine (C-X-C motif) ligand 5 (LIX) ($P<.02$); and macrophage inflammatory protein-1 gamma (MIP-1γ) ($P<.01$) in the serum compared to untreated tumor-bearing mice (Supplementary Figure S1). Soluble tumor necrosis factor receptor superfamily member 1Ab (sTNFRII) levels were not significantly different ($P>.08$) in treated and untreated mice. Taken together, these data suggest that reduced tumor burden from trabectedin treatment in the clinical skeletal metastasis model may be a result of the modulation of protumorigenic mononuclear cells and proinflammatory cytokines.

Modulation of Bone Marrow–Derived Macrophages by Trabectedin

Previously, trabectedin has been shown to induce apoptosis via activation of caspase 8 by targeting TRAILR2-positive cells, which include both M1 and M2 cells [11]. In the current study, a consistent decrease in M2-like macrophages and a specific decrease in CD115 positive cells that correlated with an M2 phenotype were found. To further explore this relationship, bone marrow–derived macrophages were polarized to into M1 or M2 phenotypes *in vitro* and subsequently treated with trabectedin to determine cell numbers and the resultant levels of TRAILR2 and CD115. IL-4–treated and enriched M2 macrophages were more susceptible to trabectedin treatment than M1 macrophages *in vitro* (Figure 6*A*). There were no significant differences in the number of TRAILR2-positive cells between non–trabectedin-treated M1 and M2 populations, and both populations responded similarly to trabectedin, which suggest the presence of another potential target for trabectedin in the context of M1 vs. M2 differential responses (Figure 6*B*). As CD115 (CSF-1R) has been associated with an M2 phenotype [26–29], CD115 expression in polarized macrophage populations was analyzed using flow cytometry. IL-4–treated M2-enriched macrophages presented a significantly higher number of CD115 positive cells than IFNγ-treated M1-enriched macrophages (Figure 6*C*). There was no significant difference in TRAILR2 protein levels in M1 and M2 macrophages (Figure 6*D*). A similar trend was identified in CD115 protein levels with IL-4 treated M2 polarized macrophages (Figure 6*E*). Since monocyte/macrophages expressing both TRAILR2 and CD115 are progenitors to osteoclasts and are key effector cells in the bone, further analysis of the effect of trabectedin on osteoclasts was performed. After osteoclast expansion with RANKL (day 7), cells were treated with trabectedin for 24 hours. Osteoclasts were significantly reduced in number relative to controls (Figure 6*F*). Taken together, these results show that trabectedin targets not only TRAILR2-positive cells (M1 and M2 macrophages) but also CD115-positive cells. Moreover, a trabectedin effect on M2 macrophages may be preferential due to the increased expression of CD115 in M2, resulting in sustained suppression of M2 macrophage levels.

Discussion

Enhanced macrophage density in tumors is associated with a poor prognosis. Tumor-associated monocytes and macrophages have been shown to correlate with a protumorigenic, anti-inflammatory response [3,4,30]. Despite such findings in primary tumors, the functional role and macrophage phenotype in the context of prostate cancer skeletal metastasis have been underexplored. Macrophages are phagocytic cells that rapidly clear apoptotic debris and assist in maintaining tissue homeostasis. Our recent study reported that prostate cancer–associated macrophage efferocytosis induced an M2 polarization of macrophages *in vitro* [9]. The present study suggests that M2-like macrophage (F4/80$^+$CD206$^+$) efferocytosis is a critical cellular function which enhances prostate cancer cell growth.

Currently, there is no curative treatment for prostate cancer bone metastasis, and consequently, over 90% of patients that die from prostate cancer have bone involvement [31]. Tumor recurrence in patients having received prior chemotherapeutic treatment can be problematic due to drug effects on cells other than tumor cells in the bone/bone marrow environment. For example, cyclophosphamide, a common chemotherapeutic drug, enhanced experimental prostate cancer skeletal metastasis in association with an increase in other myeloid effector cells that supported tumor growth [25]. Interestingly, trabectedin, a novel and recently FDA-

Figure 3. Ablation of M2-like bone marrow cells retards prostate cancer tumor growth. (A) Schematic representation of the experimental design (preventative pretreatment regimen). Male athymic mice were divided into two groups and treated with a single injection of saline control ($n=10$) or trabectedin ($n=8$). Seven days after initial treatment (0.15 kg/mg/bodyweight), PC-3^{Luc} cells were injected into the bone marrow space of both the left and right tibiae, and mice were followed for 42 days. (B) Tumor growth in the hind limbs was measured weekly using bioluminescence. *$P<.05$ vs. vehicle. (C) Whole blood was collected, and monocytes were isolated and analyzed with flow cytometry for CD11b, CD45, and CD115 (with representative flow cytometric analyses). Data are mean ± SE, *$P<.05$ vs. vehicle. (D) Bone marrow cells were isolated and analyzed for markers F4/80, CD68, CD86, and CD206 using flow cytometric analysis (with representative flow cytometric analyses). Data are mean ± SE, *$P<.05$ vs. vehicle.

approved chemotherapeutic drug for the clinical treatment of sarcomas, has been shown to target phagocytic cells and induce apoptosis via caspase-8 activation [11]. While this mechanism has been approved for soft-tissue sarcomas and use in prostate cancer is being explored in clinical trials [32], the exact mechanism has not been well defined. This study showed for the first time that modulation of the bone microenvironment

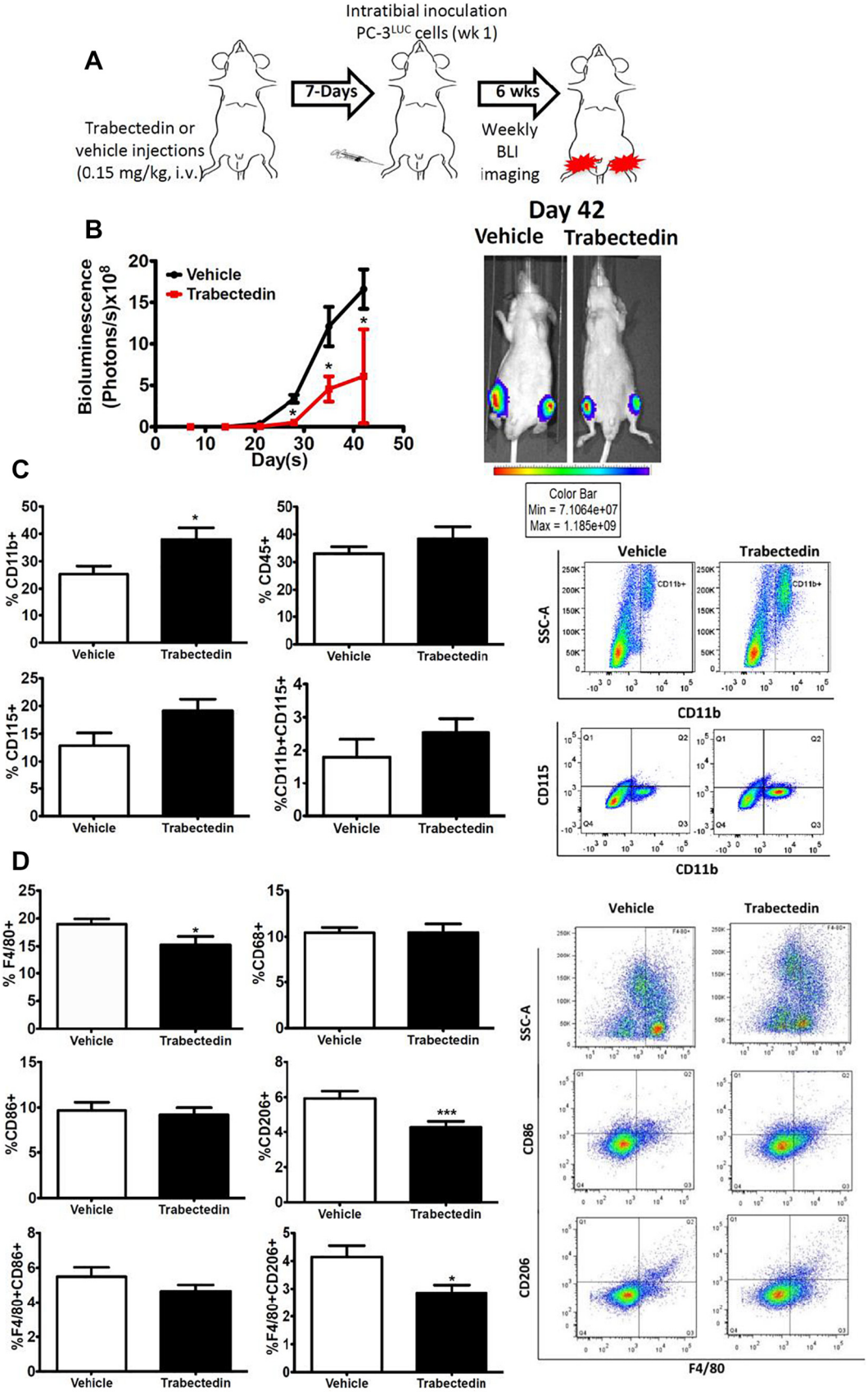

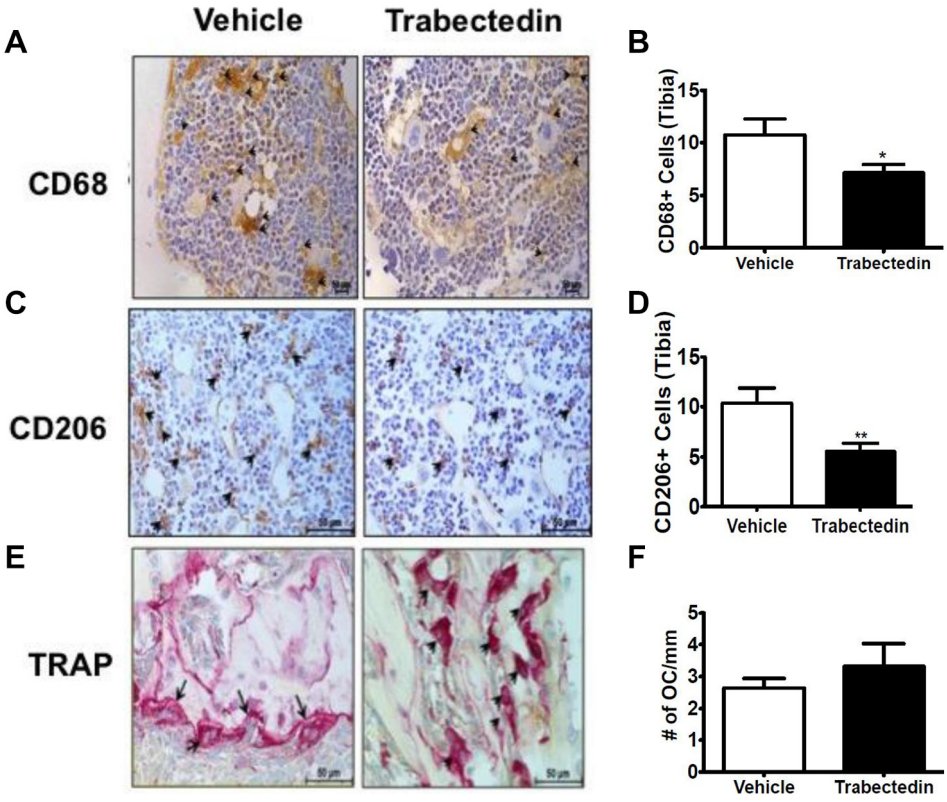

Figure 4. Immunohistochemistry of trabectedin-treated murine intratibial prostate tumors. Immunohistochemistry was performed on orthotopic tibial sections of vehicle- ($n=10$) and trabectedin- ($n=8$) treated mice as described in Figure 3. Representative images are at 400× magnification. Staining was quantified by counting three different fields of view per specimen. Arrows indicate positive cells. Data are mean ± SE. (A-B) Representative CD68 staining and quantitative analysis, *$P<.05$ vs. vehicle. (C-D) Representative CD206 staining and quantitative analysis,**$P<.01$ vs. vehicle. (E-F) Representative TRAP staining and quantification of positive osteoclastic cells (indicated by arrows) per mm of bone. There was no significant difference in osteoclast numbers.

by trabectedin preferentially reduced M2 macrophages and decreased tumor burden in the skeleton.

This study highlights both "therapeutic" and "preventative" treatment regimens which collectively highlight the importance of targeting M2-like macrophages in the bone microenvironment on PCa skeletal metastatic outcomes. In a "therapeutic" trabectedin treatment regimen, trabectedin was given biweekly *after* intracardiac injection of PC-3 cells and shown to reduce tumor size. While the reduced tumor size is likely due in part to direct effects of trabectedin on the injected PC-3 cells, it is also likely that part of the reduced tumor burden is due to inhibition of macrophages which have been previously implicated in prostate cancer metastatic outcomes [23]. Moreover, the reduced tumor size could be due to reduced prostate cancer cell growth, increased apoptosis, or both. The "preventative" trabectedin treatment regimen helps isolate the impact of bone marrow M2-like macrophages and the bone microenvironment on prostate cancer growth in the skeleton. Trabectedin, which has a half-life of under a day in rats, was given 7 days *before* PC-3 cell injection into the bone microenvironment in mice. While the M2 macrophage populations were reduced at the time point of PC-3 cell injection (7 days post-trabectedin), it is unlikely any trabectedin remained in the animal to directly inhibit newly injected cancer cells. Thus, the reduced tumor burden in the "preventative" trabectedin treatment regimen prior to cancer cell injection highlights the role of M2-like macrophages on prostate cancer metastatic growth. Targeting the M2-like macrophage populations with trabectedin or other macrophage targeting strategies may have beneficial outcomes.

The ability of trabectedin to target M2-like macrophages and their efferocytosis capabilities was shown to be a potential mechanism for prostate cancer skeletal metastatic tumor growth in this study. Specifically, it was shown that macrophage efferocytosis of cancer cells leads to secretion of factors that stimulate prostate cancer cell growth in controlled co-culture experiments, resulting in a potential positive feedback mechanism. While multiple factors are likely responsible for efferocytosis

Figure 5. M2-like monocytes and macrophages in experimental prostate cancer skeletal metastasis model. (A) Schematic of the experimental design (therapeutic treatment regimen). Male athymic mice were divided into two groups and were injected with PC-3^{Luc} in the left ventricle of the heart. Trabectedin was subsequently administered (0.15 kg/mg/bodyweight) in three doses: 7 days after tumor inoculation, at week 3, and at week 5. (B) Representative images of *in vivo* bioluminescence on day 42. (C) Hind limb metastatic tumor growth was measured by weekly *in vivo* bioluminescence imaging. Data are mean ± SE, **$P<.01$ vs. vehicle. (D) Mandibular metastatic tumor size was measured by weekly *in vivo* bioluminescence imaging. Data are mean ± SE, *$P<.05$ vs. vehicle. (E) Bone marrow cells were isolated and analyzed for markers F4/80, CD68, CD86, and CD206 using flow cytometric analysis (representative flow cytometric analyses at right). Data are mean ± SE, *$P<.05$, #$P<.0001$ vs. vehicle.

effect on prostate cancer cell growth, recent studies have identified CXCL5 as a key regulator of this response [7]. As M2-like macrophages were shown to be ~4-fold more capable of efferocytosis than M1-like macrophages in this study, inhibition of M2-like macrophages and efferocytosis by trabectedin may be particularly useful. Polarization to the M2- vs M1-like phenotype with IL4 and IFN-γ resulted in significantly

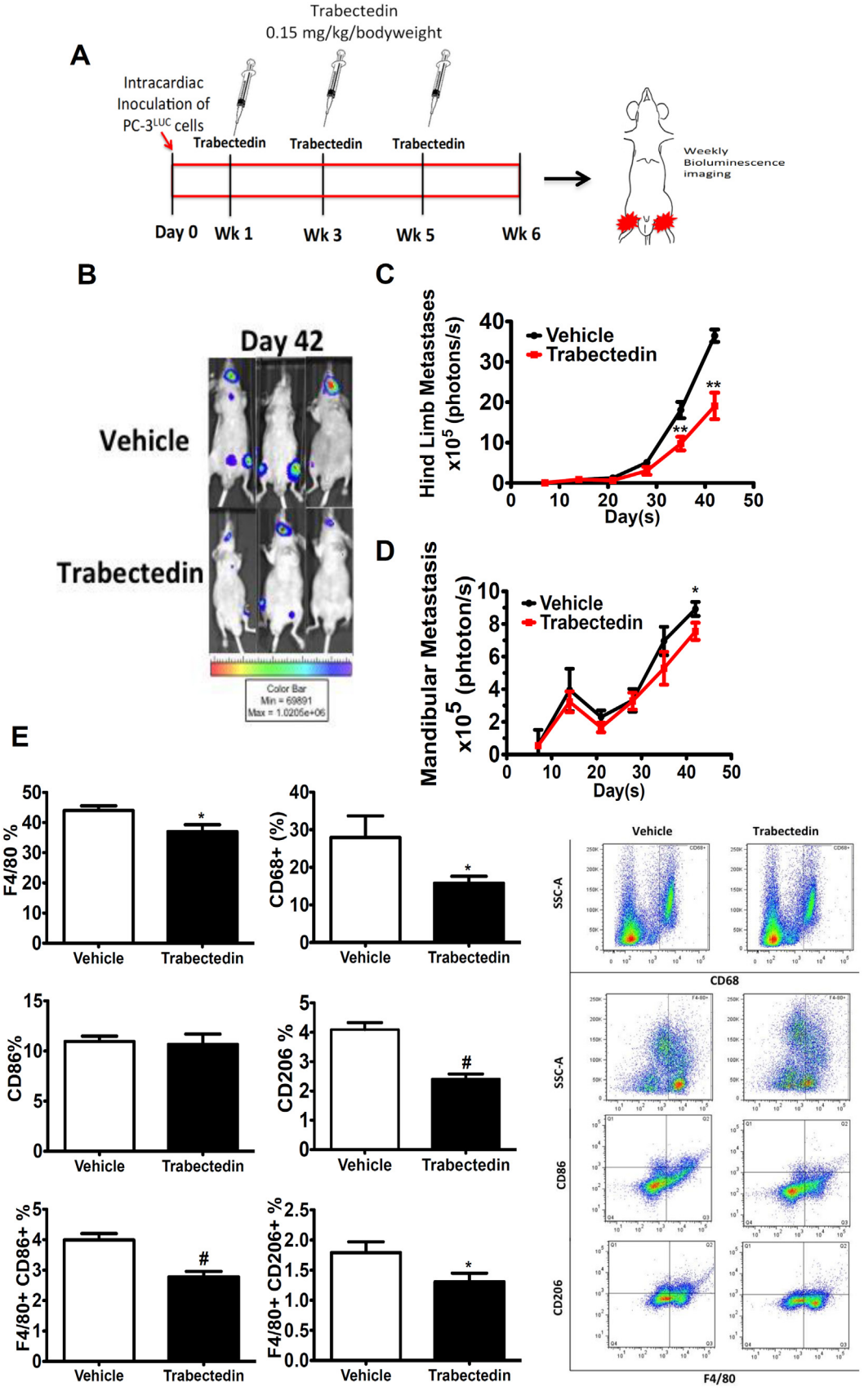

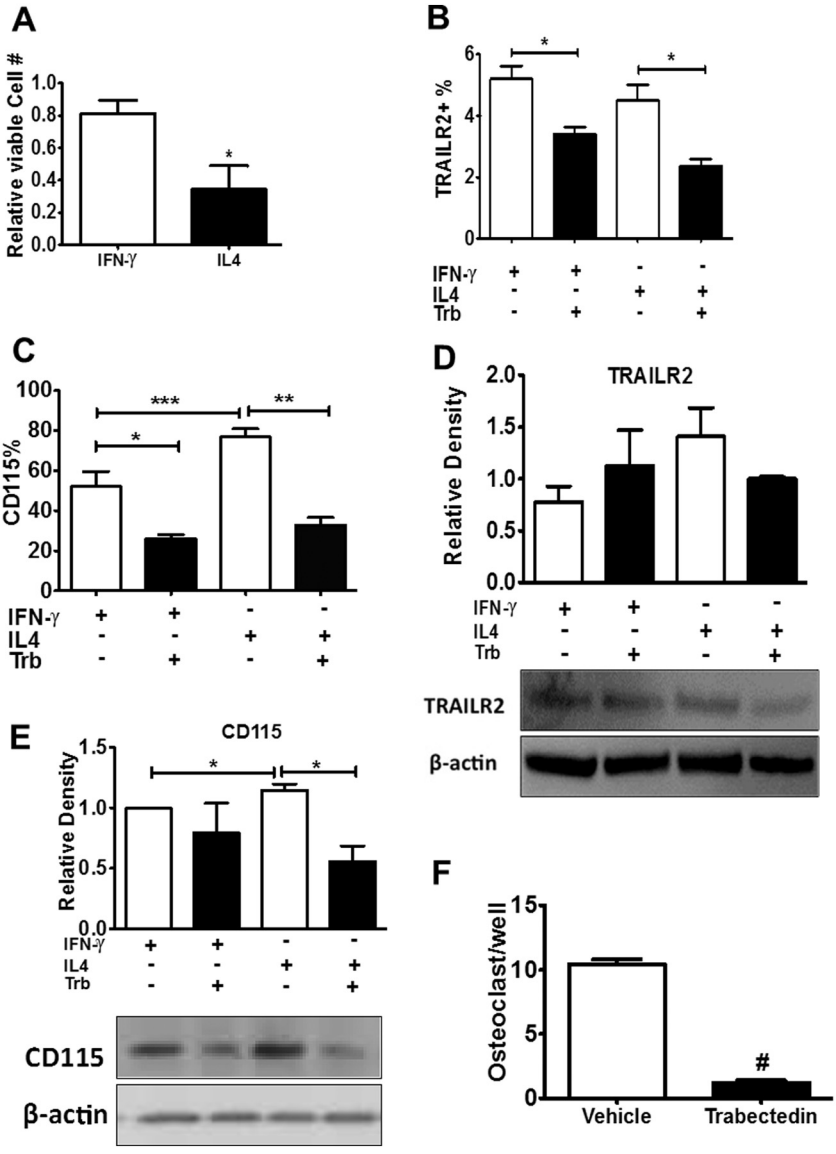

Figure 6. Modulation of polarized bone marrow–derived macrophages. (A) IL-4–treated macrophages (M2-like) were more susceptible to trabectedin treatment (10 nM) than IFN-γ treated (M1-like) *in vitro*. Viable cell numbers were normalized to untreated polarized macrophages. Data are mean ± SE (n=5/group), *P<.05. (B-C) Flow cytometric analysis of polarized macrophages untreated or treated with trabectedin *in vivo*. (B) TRAILR2$^+$; (C) CD115$^+$. Data are mean ± SE (n=4/group), *P<.05, **P<.01, ***P<.001. (D-E) Images and quantification for Western blot. (D) TRAILR2; (E) CD115. Experiments were repeated three times. Data are a mean ± SE, *P<.05. (F). Quantification of bone marrow expanded osteoclasts using RANKL, treated or untreated with trabectedin. Data are mean ± SE, #P<.0001.

greater expression of TGF-β and YM1 which are associated with a protumorigenic, anti-inflammatory response [19,20].

In this study, we observed that the phagocytic marker CD68 was positively associated with higher Gleason scores in human tumor samples, supporting a potential role of M2-like macrophages and efferocytosis in tumor growth. In humans, CD14$^+$CD16$^+$ monocytes exhibit a higher rate of phagocytosis, which is associated with acute and chronic inflammation [33]. In metastatic gastrointestinal carcinoma, patients exhibited a significant elevation in a unique CD16$^+$ monocyte population in the blood, which did not correlate with sepsis or bacterial infection [4,34]. Moreover, the presence of this monocyte subset predicted tissue invasiveness of cholangiocarcinoma and was elevated in patients with solid tumors [4,35]. Interestingly, in patients with non–small cell lung cancer, no significant difference in classical monocyte levels was found [36]. As a result, these cells tend to have a high turnover rate that may render differences more challenging to discern. In addition, patients with metastatic disease present high levels of CD115 in the blood and may recruit and stimulate polarization of macrophages to a more M2-like phenotype [37,38], further fostering an environment conducive for tumor growth. Metastatic tumor cells require CD115-positive macrophages for extravasation and growth in metastatic sites [39]. Moreover, the prostate cancer cells themselves may secrete factors such as protein kinase C zeta and MFG-E8 that may promote and M2 phenotype [9,40]. Collectively, the role of M2-like macrophages and efferocytosis is supported not only by data in this study and murine models but also by clinical observations.

Interestingly, CD11b+ cells were upregulated in the presence of a tumor with trabectedin treatment but not with trabectedin treatment

in nontumorous mice. One possibility for this discrepancy is that there is an interaction between the impact of the tumor and those of trabectedin treatment that leads to a differential effect. In addition, the trabectedin treatment history and timing are different when comparing the tumor models and to trabectedin treatment of nontumorous mice, which may also explain the observed differences.

Given the known role of trabectedin in targeting monocytes, we explored the potential effects of the agent on osteoclasts which derive from a similar lineage and contribute to prostate cancer pathophysiology [41]. Interestingly, little impact of trabectedin was observed on the number of osteoclasts *in* vivo in the tumor despite a strong *in vitro* effect on osteoclast number. The disparate *in vivo* and *in vitro* effects on osteoclasts are similar to a recent study that examined the impact of trabectedin during steady-state bone homeostasis and found no change in osteoclast surface in trabecular bone despite also identifying *in vitro* effects [42]. This may suggest that *in vivo* and around the tumor, osteoclasts are a preferentially maintained myeloid cell type.

Finally, we investigated the impact of trabectedin on bone mass in the tumor bone setting. In many bones, we observed that the primary driver of observed bone mass changes appears due to the destruction of bone by the tumor and not subtle shifts in the balance of bone remodeling. In the tibia of the direct intratibial tumor model, we found no difference in bone area per total area on histological sections with trabectedin treatment (Suppl. Figure 3*A*). In the intracardiac tumor model, we observed a significant decrease in the amount of bone in the tibia with trabectedin (Suppl. Figure 3*B*). In a prior study, we observed that, in mice without tumors, trabectedin treatment significantly reduced bone mass in the tibia [42]. The differences in bone mass between the intratibial and intracardiac tumor models could be due to several reasons. One possible explanation for this difference is that the timing and number trabectedin treatments were different between the intratibial and intracardiac models. As highlighted above, tumor itself can destroy the existing bone and may dominate any direct effects of trabectedin on the bone. Of note, the intratibial tumors are larger than the intracardiac and can lead to more bone destruction and variability than observed in the intracardiac model. Chemotherapies that directly have a negative effect on bone mass could still be beneficial to preserving bone around the tumor if they sufficiently prevent tumor growth.

In conclusion, this study showed that both "preventative" and "therapeutic" trabectedin treatment regimens are effective in preclinical models of prostate cancer. M2 (alternatively activated) monocytes and macrophages support prostate cancer skeletal metastasis, which is, in part, a result of their active engagement in efferocytosis, thus providing an anti-inflammatory environment for tumor growth. Targeting these phagocytic monocytes and macrophages with trabectedin rehabilitated the bone microenvironment by significantly decreasing M2 macrophages leading to a decrease in tumor burden. Therapies targeting these subpopulations show promise as a therapeutic approach for skeletal metastasis.

Acknowledgements

The authors thank the University of Michigan School of Dentistry histology core for assistance with histology, the University of Michigan Flow Cytometry core, Jan Berry for assistance with flow cytometry analysis, Russell Taichman for a critical read of the manuscript, and Todd Morgan and Kenneth Pienta for early feedback

Appendix A. Supplementary data

Supplementary data to this article can be found online at https://doi.org/10.1016/j.neo.2018.11.003.

References

[1] Weilbaecher KN, Guise TA, and McCauley LK (2011). Cancer to bone: a fatal attraction. *Nat Rev Cancer* **11**(6), 411–425.

[2] Sica A, Schioppa T, Mantovani A, and Allavena P (2006). Tumour-associated macrophages are a distinct M2 polarised population promoting tumour progression: potential targets of anti-cancer therapy. *Eur J Cancer* **42**(6), 717–727.

[3] Marvel D and Gabrilovich DI (2015). Myeloid-derived suppressor cells in the tumor microenvironment: expect the unexpected. *J Clin Invest* **125**(9), 3356–3364.

[4] Subimerb C, Pinlaor S, Lulitanond V, Khuntikeo N, Okada S, McGrath MS, and Wongkham S (2010). Circulating CD14+CD16+ monocyte levels predict tissue invasive character of cholangiocarcinoma. *Clin Exp Immunol* **161**(3), 471–479.

[5] Saleh MN, Goldman SJ, LoBuglio AF, Beall AC, Sabio H, McCord MC, Minasian L, Alpaugh RK, Weiner LM, and Munn DH (1995). CD16+ monocytes in patients with cancer: spontaneous elevation and pharmacologic induction by recombinant human macrophage colony-stimulating factor. *Blood* **85**(10), 2910–2917.

[6] Feng A-L, Zhu J-K, Sun J-T, Yang M-X, Neckenig MR, Wang X-W, Shao Q-Q, Song B-F, Yang Q-F, and Kong B-H, et al (2011). CD16+ monocytes in breast cancer patients: expanded by monocyte chemoattractant protein-1 and may be useful for early diagnosis. *Clin Exp Immunol* **164**(1), 57–65.

[7] Roca H, Jones JD, Purica MC, Weidner S, Koh AJ, Kuo R, Wilkinson JE, Wang Y, Daignault-Newton S, and Pienta KJ, et al (2018). Apoptosis-induced CXCL5 accelerates inflammation and growth of prostate tumor metastases in bone. *J Clin Invest* **128**(1), 248–266.

[8] Huynh M-LN, Fadok VA, and Henson PM (2002). Phosphatidylserine-dependent ingestion of apoptotic cells promotes TGF-beta1 secretion and the resolution of inflammation. *J Clin Invest* **109**(1), 41–50.

[9] Soki FN, Koh AJ, Jones JD, Kim YW, Dai J, Keller ET, Pienta KJ, Atabai K, Roca H, and McCauley LK (2014). Polarization of prostate cancer-associated macrophages is induced by milk fat globule-EGF factor 8 (MFG-E8)-mediated efferocytosis. *J Biol Chem* **289**(35), 24560–24572.

[10] Michalski MN, Koh AJ, Weidner S, Roca H, and McCauley LK (2016). Modulation of osteoblastic cell efferocytosis by bone marrow macrophages. *J Cell Biochem* **117**(12), 2697–2706.

[11] Germano G, Frapolli R, Belgiovine C, Anselmo A, Pesce S, Liguori M, Erba E, Uboldi S, Zucchetti M, and Pasqualini F, et al (2013). Role of macrophage targeting in the antitumor activity of trabectedin. *Cancer Cell* **23**(2), 249–262.

[12] Schneider A, Kalikin LM, Mattos AC, Keller ET, Allen MJ, Pienta KJ, and McCauley LK (2005). Bone turnover mediates preferential localization of prostate cancer in the skeleton. *Endocrinology* **146**(4), 1727–1736.

[13] Yamashita J, Datta NS, Chun Y-HP, Yang D-Y, Carey AA, Kreider JM, Goldstein SA, and McCauley LK (2008). Role of Bcl2 in osteoclastogenesis and PTH anabolic actions in bone. *J Bone Miner Res* **23**(5), 621–632.

[14] Koh AJ, Novince CM, Li X, Wang T, Taichman RS, and McCauley LK (2011). An irradiation-altered bone marrow microenvironment impacts anabolic actions of PTH. *Endocrinology* **152**(12), 4525–4536.

[15] Novince CM, Michalski MN, Koh AJ, Sinder BP, Entezami P, Eber MR, Pettway GJ, Rosol TJ, Wronski TJ, and Kozloff KM, et al (2012). Proteoglycan 4: a dynamic regulator of skeletogenesis and parathyroid hormone skeletal anabolism. *J Bone Miner Res* **27**(1), 11–25.

[16] Park SI, Kim SJ, McCauley LK, and Gallick GE (2010). Pre-clinical mouse models of human prostate cancer and their utility in drug discovery. *Curr Protoc Pharmacol* [Editor Board SJ Enna Ed–Chief Al, 51:14.15-14.15.27].

[17] Thiele S, Göbel A, Rachner TD, Fuessel S, Froehner M, Muders MH, Baretton GB, Bernhardt R, Jakob F, and Glüer CC, et al (2015). WNT5A has anti-prostate cancer effects in vitro and reduces tumor growth in the skeleton in vivo. *J Bone Miner Res* **30**(3), 471–480.

[18] Korns D, Frasch SC, Fernandez-Boyanapalli R, Henson PM, and Bratton DL (2011). Modulation of macrophage efferocytosis in inflammation. *Front Immunol* **2**.

[19] Raes G, De Baetselier P, Noël W, Beschin A, Brombacher F, and Hassanzadeh Gh G (2002). Differential expression of FIZZ1 and Ym1 in alternatively versus classically activated macrophages. *J Leukoc Biol* **71**(4), 597–602.

[20] Ryzhov SV, Pickup MW, Chytil A, Gorska AE, Zhang Q, Owens P, Feoktistov I, Moses HL, and Novitskiy SV (2014). Role of TGFβ signaling in generation of CD39+CD73+ myeloid cells in tumors. *J Immunol* **193**(6), 3155–3164.

[21] Perez-Ruixo JJ, Zannikos P, Hirankarn S, Stuyckens K, Ludwig EA, Soto-Matos A, Lopez-Lazaro L, and Owen JS (2007). Population pharmacokinetic meta-analysis of trabectedin (ET-743, Yondelis) in cancer patients. *Clin Pharmacokinet* **46**(10), 867–884.

[22] Reid JM, Kuffel MJ, Ruben SL, Morales JJ, Rinehart KL, Squillace DP, and Ames MM (2002). Rat and human liver cytochrome P-450 isoform metabolism of ecteinascidin 743 does not predict gender-dependent toxicity in humans. *Clin Cancer Res* **8**(9), 2952–2962.

[23] Soki FN, Cho SW, Kim YW, Jones JD, Park SI, Koh AJ, Entezami P, Daignault-Newton S, Pienta KJ, and Roca H, et al (2015). Bone marrow macrophages support prostate cancer growth in bone. *Oncotarget* **6**(34), 35782–35796.

[24] MacDonald KPA, Palmer JS, Cronau S, Seppanen E, Olver S, Raffelt NC, Kuns R, Pettit AR, Clouston A, and Wainwright B, et al (2010). An antibody against the colony-stimulating factor 1 receptor depletes the resident subset of monocytes and tissue- and tumor-associated macrophages but does not inhibit inflammation. *Blood* **116**(19), 3955–3963.

[25] Park SI, Liao J, Berry JE, Li X, Koh AJ, Michalski ME, Eber MR, Soki FN, Sadler D, and Sud S, et al (2012). Cyclophosphamide creates a receptive microenvironment for prostate cancer skeletal metastasis. *Cancer Res* **72**(10), 2522–2532.

[26] Duluc D, Delneste Y, Tan F, Moles M-P, Grimaud L, Lenoir J, Preisser L, Anegon I, Catala L, and Ifrah N, et al (2007). Tumor-associated leukemia inhibitory factor and IL-6 skew monocyte differentiation into tumor-associated macrophage-like cells. *Blood* **110**(13), 4319–4330.

[27] Haegel H, Thioudellet C, Hallet R, Geist M, Menguy T, Le Pogam F, Marchand J-B, Toh M-L, Duong V, and Calcei A, et al (2013). A unique anti-CD115 monoclonal antibody which inhibits osteolysis and skews human monocyte differentiation from M2-polarized macrophages toward dendritic cells. *MAbs* **5**(5), 736–747.

[28] Martinez MD, Schmid GJ, McKenzie JA, Ornitz DM, and Silva MJ (2010). Healing of non-displaced fractures produced by fatigue loading of the mouse ulna. *Bone* **46**(6), 1604–1612.

[29] Smith W, Feldmann M, and Londei M (1998). Human macrophages induced in vitro by macrophage colony-stimulating factor are deficient in IL-12 production. *Eur J Immunol* **28**(8), 2498–2507.

[30] Luo Y, Zhou H, Krueger J, Kaplan C, Lee S-H, Dolman C, Markowitz D, Wu W, Liu C, and Reisfeld RA, et al (2006). Targeting tumor-associated macrophages as a novel strategy against breast cancer. *J Clin Invest* **116**(8), 2132–2141.

[31] Loberg RD, Logothetis CJ, Keller ET, and Pienta KJ (2005). Pathogenesis and treatment of prostate cancer bone metastases: targeting the lethal phenotype. *J Clin Oncol* **23**(32), 8232–8241.

[32] Michaelson MD, Bellmunt J, Hudes GR, Goel S, Lee RJ, Kantoff PW, Stein CA, Lardelli P, Pardos I, and Kahatt C, et al (2012). Multicenter phase II study of trabectedin in patients with metastatic castration-resistant prostate cancer. *Ann Oncol* **23**(5), 1234–1240.

[33] Scherberich JE and Nockher WA (1999). CD14++ monocytes, CD14+/CD16+ subset and soluble CD14 as biological markers of inflammatory systemic diseases and monitoring immunosuppressive therapy. *Clin Chem Lab Med* **37**(3), 209–213.

[34] Wong KL, Tai JJ-Y, Wong W-C, Han H, Sem X, Yeap W-H, Kourilsky P, and Wong S-C (2011). Gene expression profiling reveals the defining features of the classical, intermediate, and nonclassical human monocyte subsets. *Blood* **118**(5), e16–e31.

[35] Walsh PC (2012). Re: Denosumab and bone-metastasis-free survival in men with castration-resistant prostate cancer: results of a phase 3, randomised, placebo-controlled trial. *J Urol* **187**(6), 2098.

[36] Almatroodi SA, McDonald CF, Collins AL, Darby IA, and Pouniotis DS (2014). Blood classical monocytes phenotype is not altered in primary non-small cell lung cancer. *World J Clin Oncol* **5**(5), 1078–1087.

[37] Chambers SK (2009). Role of CSF-1 in progression of epithelial ovarian cancer. *Future Oncol* **5**(9), 1429–1440.

[38] Scholl SM, Lidereau R, de la Rochefordière A, Le-Nir CC, Mosseri V, Noguès C, Pouillart P, and Stanley FR (1996). Circulating levels of the macrophage colony stimulating factor CSF-1 in primary and metastatic breast cancer patients. A pilot study. *Breast Cancer Res Treat* **39**(3), 275–283.

[39] Qian B, Deng Y, Im JH, Muschel RJ, Zou Y, Li J, Lang RA, and Pollard JW (2009). A distinct macrophage population mediates metastatic breast cancer cell extravasation, establishment and growth. *PLoS ONE* **4**(8)e6562.

[40] Fan H-H, Li L, Zhang Y-M, Yang J, Li M-C, Zeng F-Y, and Deng F (2017). PKCζ in prostate cancer cells represses the recruitment and M2 polarization of macrophages in the prostate cancer microenvironment. *Tumour Biol* **39**(6) [1010428317701442].

[41] Sinder BP, Pettit AR, and McCauley LK (2015). Macrophages: their emerging roles in bone. *J Bone Miner Res* **30**(12), 2140–2149.

[42] Sinder BP, Zweifler L, Koh AJ, Michalski MN, Hofbauer LC, Aguirre JI, Roca H, and McCauley LK (2017). Bone mass is compromised by the chemotherapeutic trabectedin in association with effects on osteoblasts and macrophage efferocytosis. *J Bone Miner Res* **32**(10), 2116–2127.